nature communications

Article

https://doi.org/10.1038/s41467-025-62288-7

Harnessing artificial intelligence to identify Bufalin as a molecular glue degrader of estrogen receptor alpha

Received: 1 October 2024

Accepted: 13 July 2025

Published online: 22 August 2025

Check for updates

Shilong Jiang[1,2,9], Keyi Liu[3,9], Ting Jiang[4,9], Hui Li[5], Xiao Wei[5], Xiaoya Wan[4], Changxin Zhong[4], Rong Gong[4], Zonglin Chen[4,6], Chan Zou[7], Qing Zhang[3], Yan Cheng[4,8] ✉ & Dongsheng Cao[5] ✉

Target identification in natural products plays a critical role in the development of innovative drugs. Bufalin, a compound derived from traditional medicines, has shown promising anti-cancer activity; however, its precise molecular mechanism of action remains unclear. Here, we employ artificial intelligence, molecular docking, and molecular dynamics simulations to elucidate the molecular mechanism of Bufalin. Using an integrated multi-predictive strategy, we identify CYP17A1, ESR1, mTOR, AR, and PRKCD as the potential targets of Bufalin. Subsequent validation via surface plasmon resonance, biotin pulldown, and thermal shift assays confirms Bufalin's direct binding to ESR1, which encodes estrogen receptor alpha (ERα). Molecular docking analyses pinpoint Bufalin's selective interaction with Arg394 on ERα. Molecular dynamic simulations further show that Bufalin acts as a molecular glue, enhancing the interaction between ERα and the E3 ligase STUB1, thereby promoting proteasomal degradation of ERα. Given the therapeutic potential of ERα degradation in overcoming endocrine resistance, we investigate the inhibitory effect of Bufalin on endocrine-resistant models and prove Bufalin reverses Tamoxifen resistance in vitro, in vivo, and in patient-derived breast cancer organoids from tamoxifen-relapsed cases. Collectively, our findings indicate that Bufalin functions as a molecular glue to degrade ERα, offering a potential therapeutic strategy for reversing Tamoxifen resistance.

Natural products are the ideal starting points for molecular design and play a pivotal role in drug discovery. Identifying the specific targets of natural compounds is crucial for the development of innovative therapies. Bufalin, an active monomer extracted from the *Chansu*, is a potent anticancer agent used clinically in China to treat various cancers[1,2]. Accumulating evidence indicates that Bufalin exerts effective anti-tumor action against lung cancer, liver cancer, colorectal cancer, and glioma[3,4]. Recent studies have demonstrated that Bufalin inhibits tumor growth, regulates metastasis, and enhances antitumor immune responses by polarizing tumor-infiltrating macrophages toward the M1 phenotype[2]. However, the molecular mechanisms underlying Bufalin's anti-tumor activity remain to be elucidated.

[1]Department of Pharmacy, Xiangya Hospital, Central South University, Changsha, China. [2]The Hunan Institute of Pharmacy Practice and Clinical Research, Changsha, Hunan, China. [3]Department of Cardiology, West China Hospital, Sichuan University, Chengdu, China. [4]Department of Pharmacy, The Second Xiangya Hospital, Central South University, Changsha, China. [5]Xiangya School of Pharmaceutical Sciences, Central South University, Changsha, China. [6]Department of General Surgery, The Second Xiangya Hospital, Central South University, Changsha, Hunan, China. [7]Center for Clinical Pharmacology, the Third Xiangya Hospital, Central South University, Changsha, China. [8]Hunan Provincial Engineering Research Centre of Translational Medicine and Innovative Drug, Changsha, China. [9]These authors contributed equally: Shilong Jiang, Keyi Liu, Ting Jiang. ✉e-mail: yancheng@csu.edu.cn; oriental-cds@163.com

Current pharmacological research suggests that Bufalin could suppress multiple signaling pathways, including Hippo-YAP, Wnt/β-Catenin, JNK, SRC3/MIF, mTOR, and MAPK, leading to apoptosis, necrosis, and autophagy in different cancer cells[3,5–8]. Therefore, identifying Bufalin's exact anti-tumor targets is critical for optimizing its therapeutic applications.

Target identification and validation in drug discovery are time-consuming and challenging procedures. Artificial intelligence (AI), which incorporates machine learning, deep learning, and network-based algorithms, has emerged as a powerful tool for predicting the potency, toxicity, and mechanism of action of compounds, thereby accelerating drug target discovery[9,10]. Previously, we developed a multi-scale system pharmacology (MSSP) method and a combinatorial target-screening strategy to explore drug-target interactions[11,12]. Recently, we established a fused multiple biological signature (FMBS) strategy to identify promising candidate targets[13]. However, the accurate identification of drug targets remains challenging.

Estrogen receptors, including ERα and ERβ, are nuclear hormone receptors that mediate the effects of estrogen by regulating gene transcription through both signal transduction and transcription factor modulation. Among the subtypes of breast cancer, nearly 70%-80% of breast cancers are ER-positive (ER+)[14–16]. Active ER signaling promotes the proliferation and survival of ER+ breast cancer cells, with oncogenesis primarily mediated through ERα, making it a key therapeutic target[17]. Endocrine therapies, including selective estrogen receptor modulators (SERMs) like Tamoxifen, selective estrogen receptor degraders (SERDs) like Fulvestrant, and aromatase inhibitors like Letrozole constitute frontline treatments for ER+ breast cancer[18–20]. Among these agents, Tamoxifen, a selective estrogen receptor modulator, acts by competitively blocking the binding of estrogen to ERα and has significantly improved prognosis in patients with ER+ breast cancer[15,21,22]. However, the therapeutic outcome of Tamoxifen is suboptimal due to the development of de novo or acquired resistance[14]. Approximately 30% of ER+ breast cancer cases recur with resistance to Tamoxifen, and this recurrence can lead to more aggressive neoplasms[23,24]. Therefore, exploring effective therapeutic strategies to reverse Tamoxifen resistance is imperative for ER+ breast cancer.

In this study, we employ AI to predict the targets of Bufalin, and confirm that Bufalin could bind to ERα and promote ERα degradation. Mechanistic investigations reveal that Bufalin functions as a molecular glue, enhancing the interaction between ERα and the ubiquitin E3 ligase STUB1, leading to the proteasomal degradation of ERα. Based on this mechanism, we evaluate the efficacy of Bufalin against Tamoxifen-resistant breast cancer cells and find that Bufalin effectively overcomes resistance in vitro, in vivo and in patient-derived organoids. Our findings not only establish Bufalin as a molecular glue for degrading ERα but also highlight its potential as a promising therapeutic candidate for the treatment of Tamoxifen-resistant breast cancer.

Results

Exploring pharmacological mechanisms of Bufalin based on a combinatorial target screening strategy

We identified the potential targets of Bufalin by integrating target prediction methods, KEGG analysis, and multitask QSAR modeling with neural networks (Fig. 1a). Initially, we employed the FMBS method along with four target prediction platforms, Swiss Target Prediction, SEA, PPB2, and ChEMBL33, to generate comprehensive and complementary prediction data (Fig. 1b). To ensure the reliability of these initial predictions, we implemented intersection criteria that narrowed down the results to 53 candidate targets (Fig. 1b). To further refine this target list and enhance the precision of our selection, KEGG enrichment analysis was conducted on 53 candidate targets (Fig. 1c). We focused on the pathways that were statistically significant and specifically related to cancer and visualized these pathways using a chord diagram to highlight their associated targets, ultimately identifying 11 key targets (Fig. 1d). Subsequently, we developed a Chemprop model[25] trained on the 11-target datasets for systematic evaluation (Fig. 1e). Using a default cutoff of 0.8, five target proteins were identified and marked as potential targets of Bufalin: CYP17A1, ESR1, mTOR, AR, and PRKCD. This multistage approach allowed for accurate prediction of Bufalin's mechanism, effectively guiding subsequent experimental validation.

Bufalin directly interacts with estrogen receptor α (ERα)

We then proceeded to experimentally validate the interaction between Bufalin and the predicted targets. Given that the association of Bufalin with mTOR and AR has been previously reported[26,27], we evaluated the binding of Bufalin to recombinant human ESR1, PRKCD, and CYP17A1 proteins using surface plasmon resonance (SPR) assays. As shown in Fig. 2a–c, SPR assays revealed that Bufalin exhibited the strongest binding affinity for ESR1 (encodes Estrogen Receptor α, ERα) (KD = 5.42E−06 M) compared to the PRKCD (PKC delta) (1.29E−02 M) and CYP17A1 (2.94E−02 M) (Table 1). To further confirm these findings, we synthesized Biotin-Bufalin conjugates, and found that Biotin-Bufalin specifically pulled down ERα in biotin-pull down assays (Fig. 2d, e). Moreover, the binding of Biotin-Bufalin with ERα was dose-dependent (Fig. 2f), and the addition of free Bufalin in cells significantly inhibited the binding of Biotin-Bufalin to ERα (Fig. 2g). Additionally, Bufalin increased the thermal stability of ERα (Fig. 2h), and the Biotin-Bufalin and ERα were colocalized in the MCF-7 cells (Fig. 2i). These results collectively demonstrate a specific and direct binding between Bufalin and the ERα protein, supporting the potential of Bufalin as a targeted agent against ERα in ER+ breast cancer.

Bufalin induces ERα degradation and suppresses its transcriptional activity

To investigate the impact of Bufalin on ERα protein levels, ER+ breast cancer cells were treated with various concentrations of Bufalin. Western blot analysis showed dose-dependent and time-dependent ERα reduction upon Bufalin treatment (Fig. 3a, b). Notably, the mRNA of ERα had no obvious change in cells exposed to Bufalin, suggesting that the downregulation of the ERα protein was not due to genetic transcription inhibition (Supplementary Fig. 1a, b).

To further validate that Bufalin functions as an ERα protein degrader, we conducted cycloheximide (CHX) chase assays. The results demonstrated that Bufalin combined with CHX significantly accelerated the degradation of ERα (Fig. 3c). Furthermore, treatment with the proteasome inhibitor MG-132 effectively prevented the Bufalin-induced decrease in ERα protein levels (Fig. 3d). We also examined ERα expression following treatment with Bufalin alongside the E1 ubiquitin-activating enzyme inhibitor MLN4924. As illustrated in Fig. 3e, MLN4924 reversed the Bufalin-mediated downregulation of ERα. In contrast, the lysosomal inhibitor hydroxychloroquine (HCQ) failed to rescue ERα levels (Fig. 3f). Additionally, co-immunoprecipitation (Co-IP) assays revealed enhanced ubiquitination of ERα in response to Bufalin treatment (Fig. 3g, h), corroborating that Bufalin induces ERα degradation predominantly through the proteasomal pathway.

Upon ligand binding, ERα undergoes dimerization and attaches to estrogen response elements (EREs) within the promoter regions of estrogen-responsive genes, thereby promoting their transcription[28]. As results thus far demonstrated that Bufalin could degrade ERα, we next assessed whether the transcriptional actions of ERα were impaired by Bufalin. The ERE luciferase assay showed that Bufalin weakened the transcriptional activity of ERα (Fig. 3i), which was corroborated by downregulation of ERα target genes, including AGR2, CCND1, GREB1, NRIP1, PGR, and SIAH2 (Fig. 3j and Supplementary Fig. 1c).

Fulvestrant is currently the FDA-approved selective estrogen receptor degrader (SERD) that induces proteasomal degradation of ERα for the treatment of ER + breast cancer[29]. Considering that Bufalin

https://doi.org/10.1038/s41467-025-62288-7

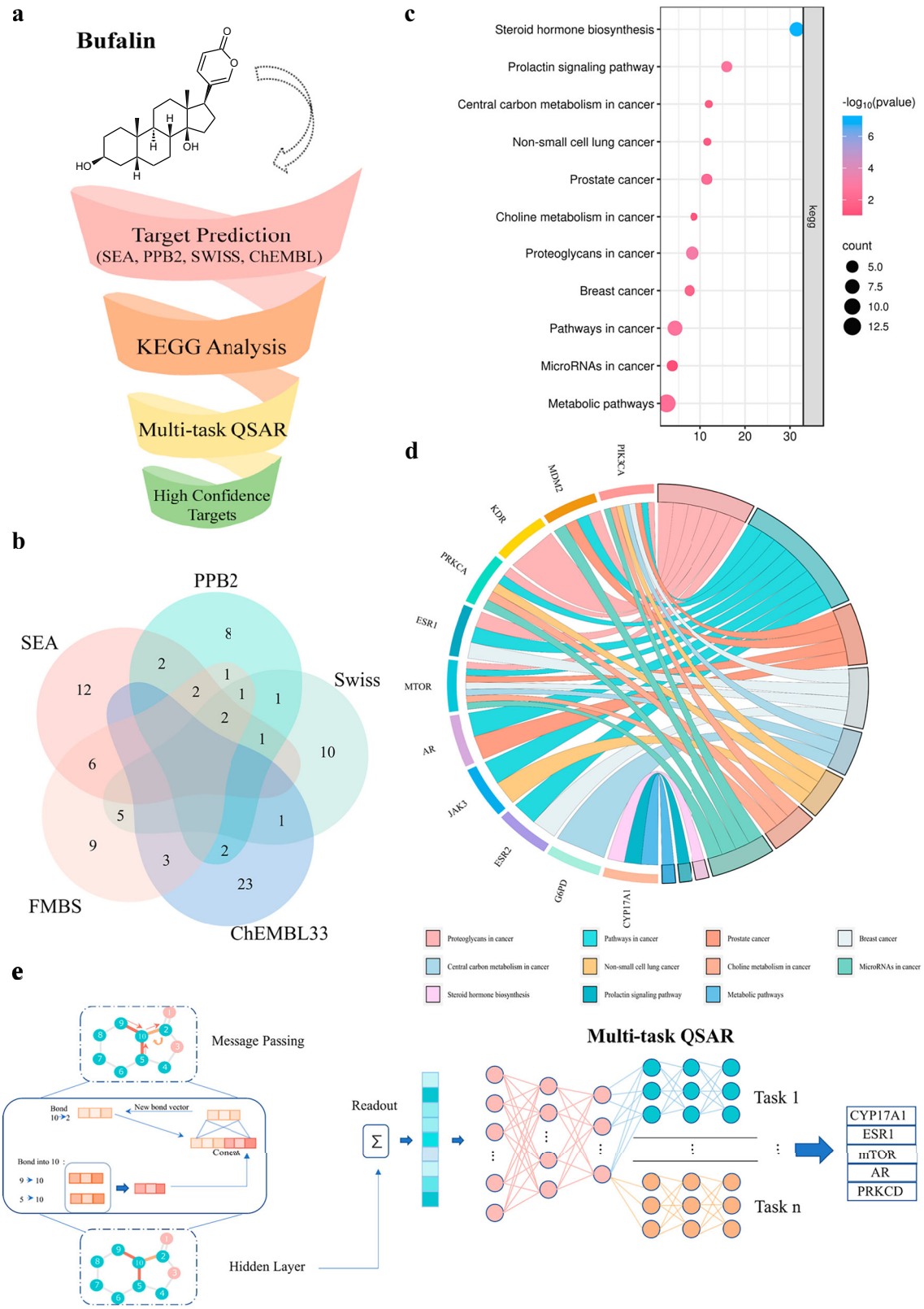

Fig. 1 | Exploring pharmacological mechanisms of Bufalin based on a combinatorial target screening strategy. a The entire process of target prediction for Bufalin. **b** Venn diagram of predicted targets by four web servers and the FMBS method. **c** Bubble chart of KEGG enrichment analysis for 53 targets. **d** Chord diagram of pathways with statistically significant *p*-values and those corresponding to cancer, as retained by KEGG analysis. This diagram illustrates these pathways and their corresponding targets, leading to the selection of 11 key targets. **e** A multi-task neural network model was developed for these 11 targets, resulting in the identification of 5 high-confidence targets: CYP17A1, ESR1, mTOR, AR, and PRKCD.

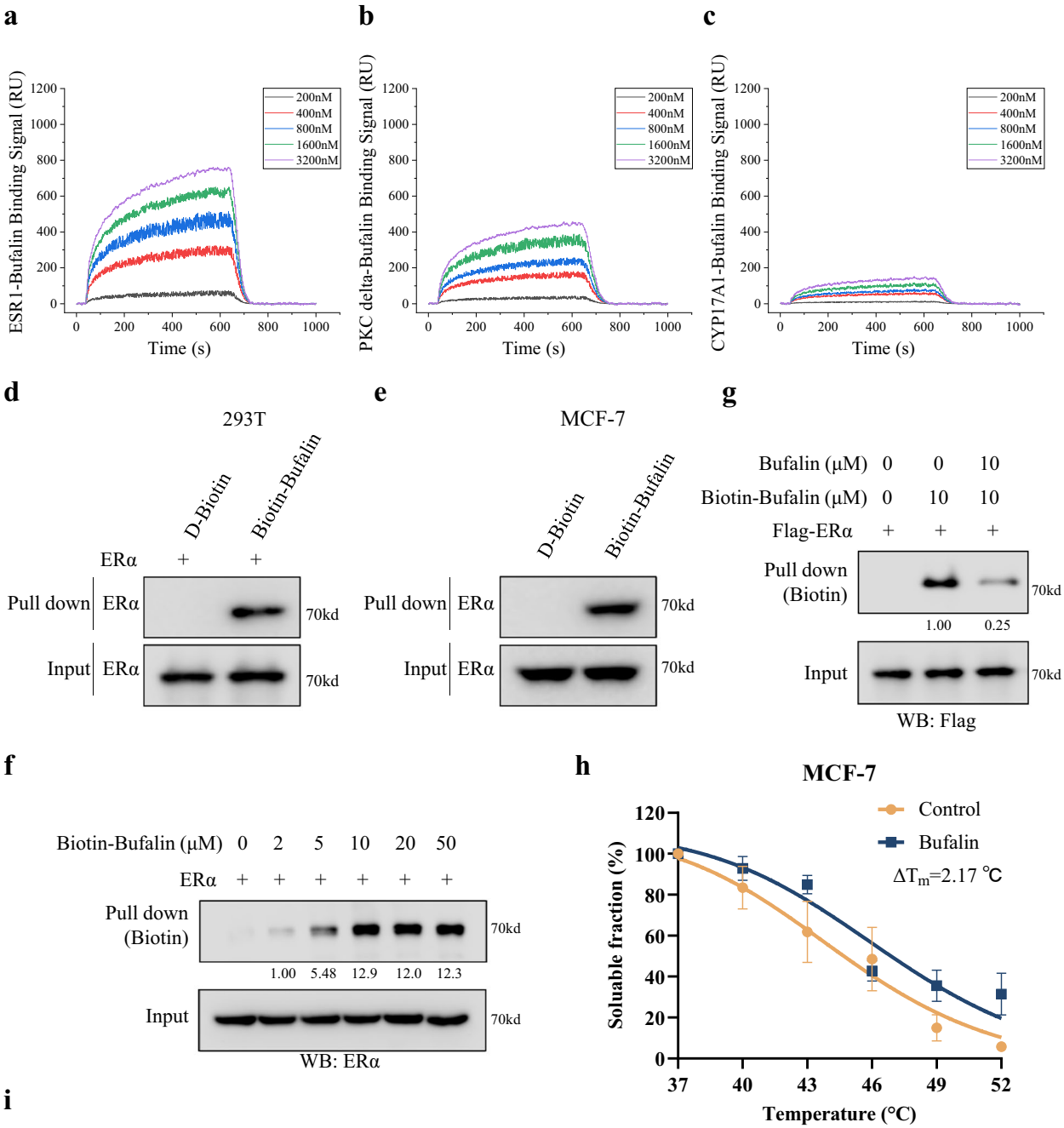

and Fulvestrant share a similar mechanism targeting ERα, we then compared the effects of each compound on ERα degradation. The results showed that Bufalin had a superior ERα degradation efficacy compared to that of Fulvestrant (Supplementary Fig. 1d). In addition, Bufalin exhibited stronger anti-cancer effects than Fulvestrant (Supplementary Fig. 1e–g). These findings highlight Bufalin as a promising therapeutic candidate with dual advantages in ERα degradation potency and anti-cancer activity.

Bufalin selectively binds to Arg394 (R394) of ERα

Next, we want to investigate the binding site of Bufalin on the protein structure of ERα. First, the Glide SP protocol was used to dock Bufalin

Fig. 2 | Bufalin directly interacts with estrogen receptor α (ERα). SPRi graph showing the interaction of Bufalin with ESR1 (**a**), PKC delta (**b**) and CYP17A1 (**c**) recombinant protein. **d** 293 T cell was transfected with ERα plasmid, after transfected 48 h, the cell lysates were incubated with D-Biotin or Biotin-Bufalin at 4 °C overnight, followed by pulling-down with streptavidin magnetic beads. The proteins bound to the magnetic beads were separated by SDS-PAGE, followed by western blot using ERα antibody. **e** MCF-7 cell lysates were incubated with D-Biotin or Biotin-Bufalin at 4 °C overnight, followed by pulling-down with streptavidin magnetic beads. The proteins bound to the magnetic beads were separated by SDS-PAGE, followed by western blot using ERα antibody. **f** 293 T cell was transfected with ERα plasmid, after transfected 48 h, the cell lysates were incubated with a series of concentrations of Biotin-Bufalin at 4 °C overnight, followed by pulling-down with streptavidin magnetic beads. The proteins bound to the magnetic beads were separated by SDS-PAGE, followed by western blot using ERα antibody. **g** 293 T cell was transfected with Flag-ERα plasmid, after transfected 48 h, the cells were incubated with Bufalin, then the cell lysates were incubated with Biotin-Bufalin at 4 °C, followed by pulling-down with streptavidin magnetic beads. The proteins bound to the magnetic beads were separated by SDS-PAGE, followed by western blot using Flag antibody. **h** The thermal shift assay experiment (CETSA) was used to evaluate the binding interaction between Bufalin and ERα, the data are presented as mean ± SD, $n = 3$ independent experiments. i. The cellular location of ERα and Biotin-Bufalin was examined by immunofluorescence staining in MCF-7 cells (Scale bar 5μm). Representative data are shown from $n = 3$ independent experiments with consistent results.

Table 1 | The kinetic parameters of Bufalin and ESR1, CYP17A1, and PKC delta binding from SPRi

Protein	Avg ka (1/Ms)	Avg kd (1/s)	Avg KD (M)	ABS (tr_KD)
ESR1	1.29E + 02	6.98E−04	5.42E−06	17.492
CYP17A1	2.50E + 00	7.36E−02	2.94E−02	5.086
PKC delta	1.79E + 01	2.31E−01	1.29E−02	6.271

into the binding pocket of ESR1 (Fig. 4a). The docked structure of the ESR1-Bufalin complex was then subjected to 100 ns molecular dynamics simulations with Amber22 software, followed by MM-GBSA energy calculations and residue energy decomposition. The top 10 residues identified from MM-GBSA energy decomposition (Fig. 4b) were further analyzed using alanine scanning mutagenesis (Fig. 4c). Our analysis revealed that residues with energy contributions better than −1 kcal/mol, specifically Leu354, Leu387, Arg394, Met528, and Ala350, are key residues for Bufalin binding to ERα.

To experimentally validate these computational findings, we generated mutant plasmids of ERα, each containing a single amino acid substitution (Leu354, Leu387, Arg394, Met528, or Ala350) with alanine or glutamine. The wild-type (WT) and mutant ERα plasmids were transfected into 293 T cells. The cell lysates were incubated with Biotin-Bufalin and subjected to pull-down experiments using streptavidin-magnetic beads. The results showed that only the ERα Arg394A mutant lost the ability to bind Biotin-Bufalin, while the other mutants retained similar binding affinities to Biotin-Bufalin compared to WT ERα (Fig. 4d). Furthermore, the degradation efficacy of Bufalin on the ERα Arg394A protein was significantly reduced (Fig. 4e). Co-IP experiments indicated a decrease in ubiquitination of the ERα Arg394A mutant compared to the WT protein in the presence of Bufalin (Fig. 4f). These findings indicate that the Arg394 residue of ERα is critical for the binding interaction between ERα and Bufalin, underscoring its importance in Bufalin-mediated ERα degradation.

Bufalin facilitates ERα degradation by enhancing interaction between ERα and the E3 ligase STUB1

Next, we investigated the molecular mechanism underlying Bufalin-induced ERα degradation. Based on the established role in the ERα-degradation pathway, we employed molecular dynamics simulation analysis to determine whether Bufalin could influence the interaction between ERα and ubiquitin ligase including TRIM56, RNF181, RNF2, and STUB1. It has been reported that the ubiquitin ligases TRIM56, RNF181, and RNF2 stabilize ERα expression[30–32]. On the contrary, the ubiquitin ligase STUB1 downregulates ERα levels through the ubiquitin–proteasome system[33]. Our results showed the binding free energy between ERα and STUB1 was changed from −4.9455 kcal/mol to −58.1918 kcal/mol owing to the involvement of Bufalin (Supplementary Table 1), consistent with the experimental results. STUB1 contains a TPR domain that specifically recognizes and binds to molecular chaperone proteins HSP70/HSP90, with ERα being a classic component of this chaperone system. Moreover, STUB1 expression is closely associated with breast cancer prognosis. Previous studies have established STUB1 as a key mediator in ERα degradation[33–35]. The Fig. 5a illustrates the binding poses of ERα and STUB1 with Bufalin: the protein-protein docking result (magenta), the clustered conformation after 200 ns MD simulation with Bufalin (green), and the clustered conformation after 200 ns MD simulation without Bufalin (blue). Detailed structural analysis of the 200 ns simulation trajectory reveals that Bufalin repositions itself deeper within the ERα binding pocket, forming a hydrogen bond with Arg394 of ERα (Fig. 5b). This repositioning appears to induce subtle conformational changes in ERα that enhance its binding interface with STUB1. RMSD analysis demonstrates that the ERα-STUB1 complex remains conformationally stable throughout the 200 ns simulation in the presence of Bufalin (Fig. 5c). This finding is further supported by the binding surface area analysis (Fig. 5d), which shows enhanced interaction between ERα and STUB1 when Bufalin is present. Moreover, RMSF profiles of ESR1 and STUB1 indicate that ligand binding reduces the flexibility of residues at the protein-protein interface. Specifically, decreased fluctuations were observed in residues 335–343, 417–425, and 515–538 of ESR1, and in residues 25–49, 61–69, and 121–136 of STUB1 (Fig. 5e). As the simulation progressed, the presence of Bufalin also resulted in an increased number of hydrogen bonds between STUB1 and ESR1, further stabilizing their interaction (Fig. 5f).

Subsequently, we sought to examine the binding between ERα and STUB1 after treatment with Bufalin. Consistent with previously published research, silencing STUB1 increased ERα levels (Fig. 5g). To determine whether STUB1 participates in Bufalin-induced ERα ubiquitination and degradation, we conducted co-immunoprecipitation (Co-IP) assays to assess the interaction between ERα and STUB1. The results showed that Bufalin enhanced the binding of ERα and STUB1 (Fig. 5h). Furthermore, STUB1 knockdown attenuated Bufalin-induced ERα degradation (Fig. 5i), suggesting that STUB1 was required for ubiquitination of ERα induced by Bufalin. Collectively, these findings suggest that Bufalin functions as a molecular glue, facilitating the interaction between ERα and STUB1 and thereby inducing proteasomal degradation of ERα.

Bufalin's anti-cancer effects in ER+ cells are dependent on ERα

To further elucidate the connection between Bufalin-mediated anti-cancer activity and ERα levels in ER+ breast cancer cells, we assessed Bufalin's impacts on cell proliferation and apoptosis. Bufalin significantly inhibited MCF-7 and T47D cells growth, as demonstrated by both colony formation and CCK-8 assays (Fig. 6a, b). Additionally, treatment with Bufalin induced apoptosis, as evidenced by the elevated Annexin V-positive populations (Fig. 6c).

To determine if Bufalin's anti-tumor effects are linked to ERα expression, ERα-knockdown models revealed a diminished therapeutic response to Bufalin, as indicated by decreased Annexin V staining (Fig. 6d, e). Moreover, ERα silencing attenuated Bufalin-induced apoptosis, which was confirmed by the reduced expression of cleaved PARP (Fig. 6f). We also observed that silencing ERα expression diminished Bufalin's anti-cancer effects on breast cancer cells (Fig. 6g),

https://doi.org/10.1038/s41467-025-62288-7

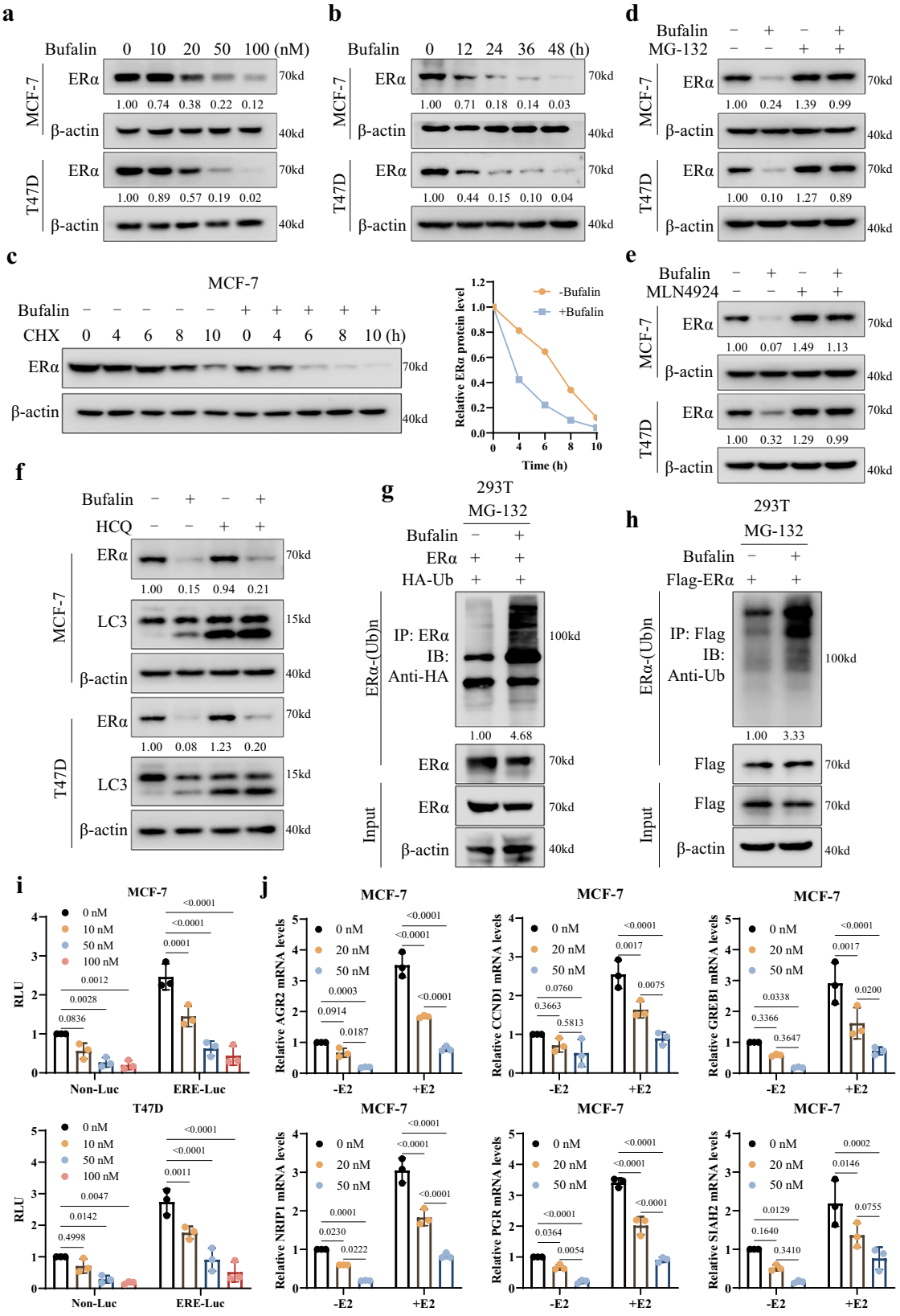

whereas cells overexpressing ERα were more sensitive to Bufalin (Fig. 6h). Consistently, colony formation assays demonstrated that cells with silenced ERα were less sensitive to Bufalin treatment compared to control cells (Fig. 6i). These findings suggest that the antitumor activity of Bufalin mechanistically depends on ERα degradation, identifying ERα as the critical therapeutic target of Bufalin.

Bufalin overcomes Tamoxifen resistance in vitro and in vivo

It has been reported that persistent ERα expression post-Tamoxifen therapy motivates SERD development, such as Fulvestrant, which improved clinical benefits after failure of other endocrine therapies[36]. Given the ERα-degradation capacity of Bufalin, we investigated Bufalin potential against endocrine resistance. Clinical

Fig. 3 | Bufalin induces ERα degradation and suppresses its transcriptional activity. a MCF-7 and T47D cells were treated with a series of concentrations of Bufalin for 48 h, and the expression of ERα was measured by western blot. **b** MCF-7 and T47D cells were treated with 50 nM Bufalin for different periods of time, and the expression of ERα was measured by western blot. **c** MCF-7 cells were treated with Bufalin, and then subjected to cycloheximide (CHX) (10 μg/ml) chase at the indicated time, the expression of ERα was measured by western blot. Representative data are shown from n = 3 independent experiments with consistent results. **d** MCF-7 and T47D cells were treated with Bufalin for 48 h with or without MG-132. The expression of ERα was measured by western blot. **e** MCF-7 and T47D cells were treated with Bufalin for 48 h in the presence or absence of MLN4924. The expression of ERα was measured by western blot. **f** MCF-7 and T47D cells were treated with Bufalin in the presence or absence of hydroxychloroquine (HCQ). The expression of ERα and LC3 was measured by western blot, the samples derive from the same experiment, and the gels/blots were processed in parallel. **g** 293 T cells were transfected with ERα plasmid and HA-Ub plasmid, and then subjected to Bufalin for 48 h, followed by treatment with MG-132 (10 μM) for 10 hours before harvest. Then the cells lysates were subjected immunoprecipitation with anti-ERα antibodies and blotted with anti-HA antibodies. **h** 293 T cells were transfected with Flag-ERα plasmid, and then subjected to Bufalin for 48 h, followed by treatment with MG-132 (10 μM) for 10 hours before harvest. Then the cells lysates were subjected immunoprecipitation with anti-Flag antibodies and blotted with anti-Ub antibodies. **i** ERE-luciferase assay after Bufalin treatment, the data are presented as mean ± SD, $n = 3$ independent experiments. Two-way ANOVA was used for statistical analysis, $P < 0.05$ was considered to be statistically significant. **j** MCF-7 cells were treated with a series of concentrations of Bufalin for 48 h in the presence or absence of E2, the mRNA levels of AGR2, CCND1, GREB1, NRIP1, PGR, and SIAH2 were analyzed by real-time PCR, the data are presented as mean ± SD, $n = 3$ independent experiments. Two-way ANOVA was used for statistical analysis, $P < 0.05$ was considered to be statistically significant.

samples from endocrine therapy-relapsed patients ($n = 8$) maintained ERα expression (Fig. 7a). We next examined the ERα proteasomal degradation by Bufalin in Tamoxifen resistance cell LCC2. As shown in Fig. 7b, the Bufalin could promote the ERα degradation in Tamoxifen-resistant cell LCC2, which suggested that the Tamoxifen-treated relapsed patient may benefit from Bufalin treatment. As shown in Fig. 7c, Bufalin treatment reduced the viability of LCC2 cells in a dose-dependent manner, with colony formation and EdU assays further confirming its inhibitory effect on cell proliferation (Fig. 7d, e). Additionally, the activation of apoptosis induced by Bufalin was evidenced by increased Annexin V staining, PARP cleavage, and Bcl-2 downregulation in LCC2 cells (Fig. 7f, g). Moreover, Bufalin exhibited better anti-cancer effects than Fulvestrant against LCC2 cells (Fig. 7h, i).

To validate the efficacy of Bufalin against Tamoxifen resistance in vivo, we established Tamoxifen-resistant LCC2 xenografts. As shown in Fig. 8a–c, following intraperitoneal injection of Bufalin, the tumor volumes and weights significantly decreased, demonstrating superior anti-tumor activity to Fulvestrant. Immunohistochemical analysis revealed marked Ki67 suppression in Bufalin-treated tumors (Fig. 8d). H&E staining revealed that xenograft tumor cells treated with Bufalin appeared more loosely arranged and exhibited smaller nuclei compared to those in the vehicle-treated group (Fig. 8e). Moreover, the protein expression of ERα was decreased in tumors following Bufalin treatment (Fig. 8f, g). To evaluate potential toxicity, we analyzed various serum biochemical markers related to liver and kidney function in mice, and found no significant signs of drug-induced toxicity at the therapeutic doses of Bufalin (Fig. 8h, i), suggesting a favorable safety profile. Taken together, these results indicate that Bufalin acts as a molecular glue-type ERα degrader that effectively overcomes Tamoxifen resistance in preclinical models.

Bufalin exerts significant anti-cancer activity in Tamoxifen-resistant patient-derived organoids

To further evaluate the therapeutic potential of Bufalin in a clinically relevant setting, we established Tamoxifen-resistant patient-derived organoids (PDOs) from relapsed breast cancer specimens. As shown in Fig. 9a, PDOs were successfully established from Tamoxifen-resistant patient specimens, and treatment with Bufalin resulted in a significant reduction in the size of these organoids, indicating its potent inhibitory effect on the growth of Tamoxifen-resistant tumors (Fig. 9b). Additionally, the Tamoxifen-resistant PDOs showed a marked decrease in cell viability after Bufalin treatment (Fig. 9c). Calcein-AM/PI fluorescence staining further revealed extensive cell death in the Bufalin-treated organoids (Fig. 9d). These results underscore the potential of Bufalin as an effective therapeutic agent for Tamoxifen resistance in ER + breast cancer and validate its translational potential in cancer therapy.

Discussion

Bufalin has emerged as a clinically validated natural compound with therapeutic potential across multiple cancer types. Mechanistic studies reveal its pleiotropic anti-tumor effects through cancer-type-specific targets[5,37]. Accordingly, identifying the molecular targets of Bufalin is pivotal for advancing drug development and repurposing efforts. To this end, various computational models for target prediction have been developed, leading to notable improvements in predictive accuracy and efficiency[38–40]. Our prior work has successfully developed a variety of strategies to predict drug targets by integrating multiple biological signatures[13], and successfully discovered the target of Ixabepilone, Mitoxantrone, and Tubeimoside-1 are Bcl-2, eEF2K, and AKT, respectively[12,41,42]. In this study, we applied an integrated multi-predictive strategy and identified CYP17A1, ESR1, mTOR, AR, and PRKCD as potential targets of Bufalin, with experimental validation confirming ERα (ESR1) as the primary target in ER+ breast cancer, offering a strategy for clinical application. Molecular docking experiments revealed that Bufalin selectively binds to R394 of ERα, while molecular dynamics simulations suggest its molecular glue function stabilizes the interaction between ERα and STUB1, leading to ERα degradation and overcoming endocrine resistance (Fig. 9e). This integrative AI strategy establishes a robust paradigm for natural product target discovery and mechanistic elucidation.

Bufalin has been reported to inhibit key signaling pathways such as mTOR, Wnt/β-catenin, and Akt, which are necessary for cancer cell survival, proliferation, and migration[3]. Furthermore, Bufalin has been shown to downregulate the expression of transcriptional coactivators SRC-1 and SRC-3, as well as the nuclear transcription factor E2F1[8,43]. Bufalin induced apoptosis, necroptosis, ferroptosis, autophagy, and senescence through AMPK, RIP1/ROS, DECR1, p62, and p53 pathways[5,44–48]. Recent studies indicated that Bufalin played an important role in the tumor microenvironment by inducing the activation of the NF-κB pathway[2]. Bufalin also appears to regulate particular non-coding RNAs, including microRNA-203 (miR-203), to suppress tumor cell proliferation[49]. Here, we found that Bufalin may serve as a molecular glue that strengthens the ERα-STUB1 interaction, thereby driving the degradation of ERα. Previous studies have reported that Bufalin exerts anti-tumor effects by inhibiting SRC in MCF-7 cells[8]. However, compared to SRC, the ERα constitutes the central oncogenic driver in ER+ breast cancer, as ERα overexpression promotes tumorigenesis[50,51]. Targeting ERα signaling is widely regarded as the most effective therapeutic strategy for ERα-positive breast cancer, such as Tamoxifen, Fulvestrant, and Letrozole, which have brought significant prognostic improvements for ER+ breast cancer[52]. Our research uncovers a promising ERα-targeting therapeutic strategy by demonstrating that Bufalin can selectively induce the degradation of ERα.

Our results demonstrate Bufalin-induced ERα degradation drives its anticancer activity, suggesting selective cytotoxicity in ERα-expressing malignancies, including cervical and colorectal cancers.

https://doi.org/10.1038/s41467-025-62288-7

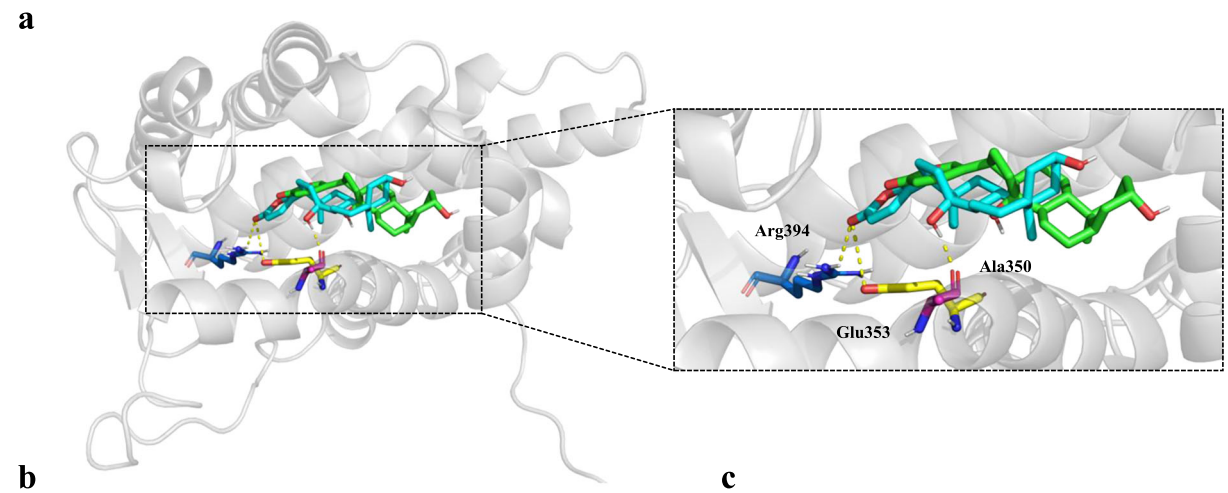

b

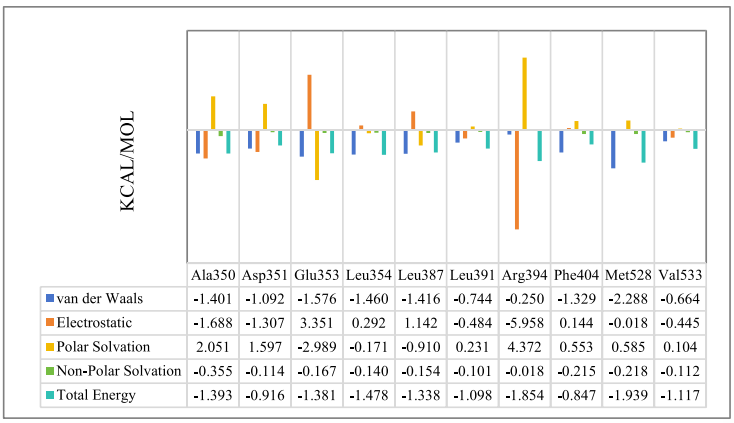

	Ala350	Asp351	Glu353	Leu354	Leu387	Leu391	Arg394	Phe404	Met528	Val533
van der Waals	-1.401	-1.092	-1.576	-1.460	-1.416	-0.744	-0.250	-1.329	-2.288	-0.664
Electrostatic	-1.688	-1.307	3.351	0.292	1.142	-0.484	-5.958	0.144	-0.018	-0.445
Polar Solvation	2.051	1.597	-2.989	-0.171	-0.910	0.231	4.372	0.553	0.585	0.104
Non-Polar Solvation	-0.355	-0.114	-0.167	-0.140	-0.154	-0.101	-0.018	-0.215	-0.218	-0.112
Total Energy	-1.393	-0.916	-1.381	-1.478	-1.338	-1.098	-1.854	-0.847	-1.939	-1.117

c

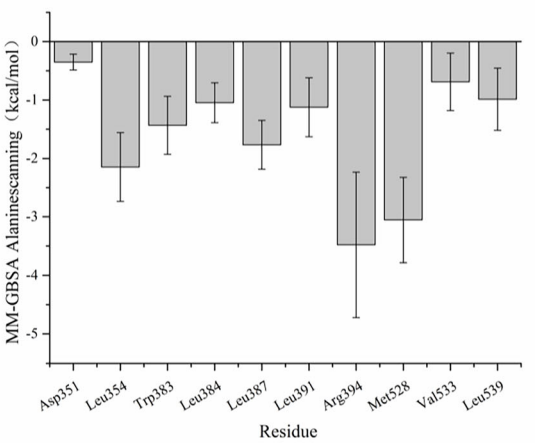

d

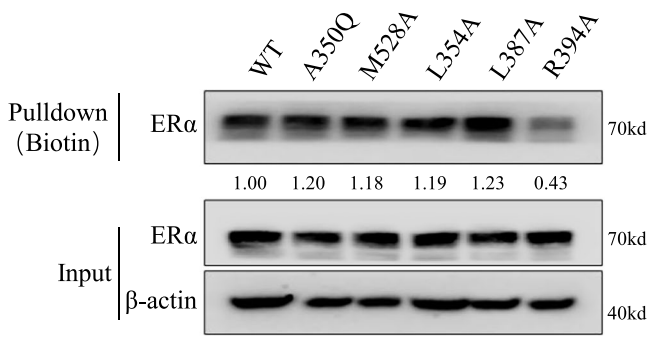

e

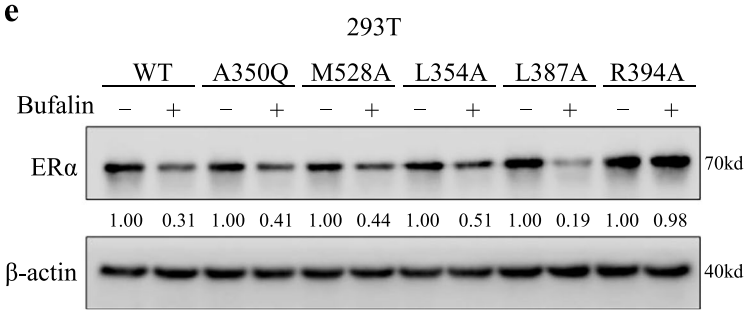

f

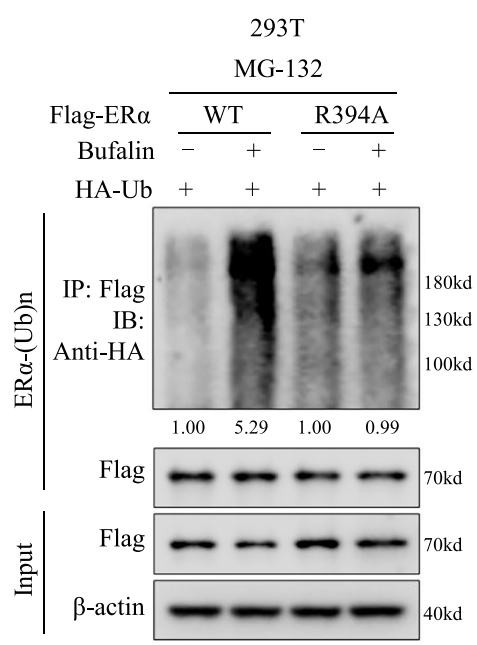

Fig. 4 | Bufalin selectively binds to Arg394 (R394) of ERα. a Bufalin was docked into the binding pocket of ESR1 using the Glide SP protocol. **b** The docked structure of the ESR1-Bufalin complex was then subjected to 100 ns of molecular dynamics simulations using Amber, followed by MM-GBSA energy calculations and residue energy decomposition. The top 10 residues from the MM-GBSA residue energy decomposition scoring. **c** The top 10 residues selected for alanine scanning mutagenesis. Error values were derived from energy snapshots based on 100 frames uniformly extracted from the last 100 ns of the MD simulation trajectory. **d** 293 T cell was transfected with ERα wild type (WT) plasmid or mutant plasmid, after transfected 48 h, the cell lysates were incubated with Biotin-Bufalin at 4 °C overnight, followed by pulling-down with streptavidin magnetic beads. The proteins bound to the magnetic beads were separated by SDS-PAGE, followed by western blot using ERα antibody. **e** 293 T cells were transfected with ERα WT or mutant plasmid, followed by treatment with Bufalin for 48 h. The ERα protein levels were measured by western blot. **f** 293 T cells were transfected with Flag-ERα WT or R394A mutant plasmid and HA-Ub plasmid, and then subjected to Bufalin for 48 h, followed by treatment with MG-132 (10 μM) for 10 hours before harvest. Then the cells lysates were subjected immunoprecipitation with anti-Flag antibodies and blotted with anti-HA antibodies.

https://doi.org/10.1038/s41467-025-62288-7

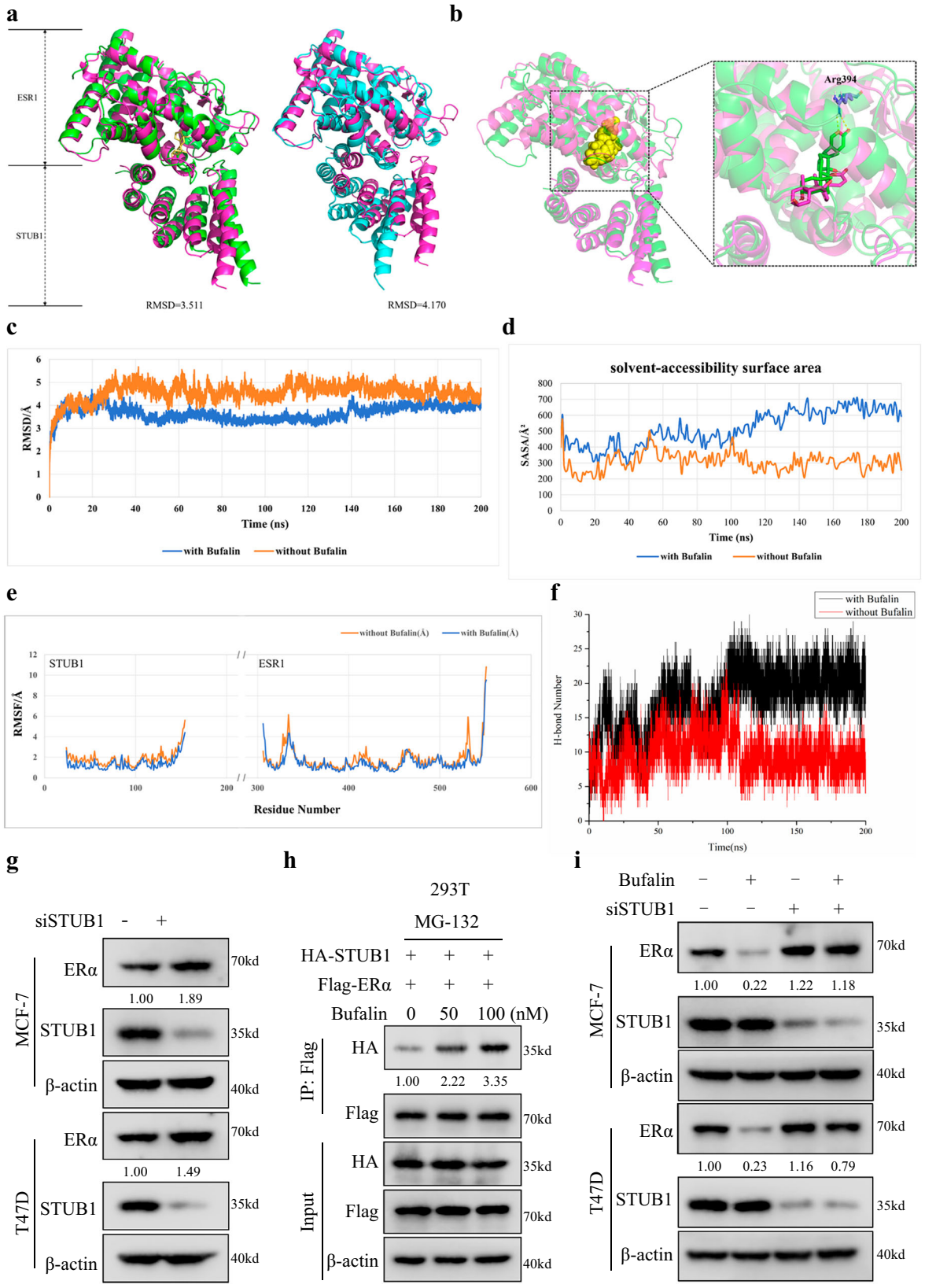

Structural analysis revealed that Bufalin could selectively bind to the R394 of the ERα protein and effectively inhibited the estrogen response elements transcriptional activity. These findings, on one hand, clarified the anti-tumor target of Bufalin with defined binding residues for molecular optimization, on the other hand, provided an experimental basis for expanding the range of possible future applications of Bufalin.

Targeted protein degradation (TPD), including molecular glues and PROTACs, has emerged as a promising strategy to target proteins previously considered undruggable[53]. Unlike conventional inhibitors,

Fig. 5 | Bufalin facilitates ERα degradation by enhancing interaction between ERα and the E3 ligase STUB1. a The binding poses of ERα and STUB1 with or without Bufalin. The magenta structure represents the result of protein-protein docking, the green structure corresponds to the clustered conformation after a 200 ns MD simulation with Bufalin, and the blue structure represents the clustered conformation after a 200 ns MD simulation without Bufalin. Bufalin is shown as yellow sticks in the structural representation. **b** The conformational changes of the ERα-Bufalin-STUB1 complex at 200 ns. **c** RMSD plots of the ERα-STUB1 complex over 200 ns of MD simulation with or without Bufalin. **d** The binding surface area analysis between ERα and STUB1 with or without Bufalin. **e** RMSF (root-mean-square fluctuation) profiles of ERα and STUB1 with or without Bufalin. **f** Changes in the number of H-bonds throughout the simulation between ERα and STUB1 with or without Bufalin. **g** MCF-7 and T47D cell was transfected with nontargeting siRNA or STUB1-targeted siRNA, the expression of ERα and STUB1 were measured by western blot, the samples derive from the same experiment and that gels/blots were processed in parallel. **h** 293 T cells transfected with Flag-ERα and HA-STUB1 plasmid were treated by Bufalin, then lysed and lysates were subjected immunoprecipitation with anti-Flag antibodies. Proteins retained on sepharose were blotted with the indicated antibodies. The input samples derive from the same experiment, and that gels/blots were processed in parallel. **i** MCF-7 and T47D cells were transfected with nontargeting siRNA or STUB1-targeted siRNA followed by treatment with Bufalin for 48 h. The ERα and STUB1 protein levels were measured by Western blot.

molecular glues facilitate protein degradation by inducing proximity between the target and E3 ligases and have gained attention as a potential strategy for targeting proteins[54,55]. Numerous small molecules have entered the clinical research stage. Previous research has revealed that Bufalin as a molecular glue that targets E2F2 and inhibits the growth of hepatoma[56]. Here, we demonstrate that Bufalin enhances ERα's association with the ubiquitin E3 ligase STUB1 by acting as a molecular glue, which results in proteasome-mediated degradation of ERα. Our study expands insights into molecular glues and provides a structural foundation for the development of structure-guided Bufalin derivatives.

Although Tamoxifen remains the standard first-line treatment for ER-positive breast cancer and has significantly improved patient prognosis, the development of acquired resistance continues to pose a major clinical challenge[57]. Therefore, how to improve the therapeutic effect of Tamoxifen and reverse resistance has been extensively investigated. An increasing number of endocrine-resistance mechanisms have been characterized, and several small molecules have been reported to overcome Tamoxifen resistance[58,59]. Our previous study has reported that the UCH-L1 inhibitor LDN significantly enhanced the efficacy of Tamoxifen both in vivo and in vitro[21]. Fulvestrant is a standard therapeutic option for endocrine-resistant or advanced metastatic ER+ breast cancer[59,60]. In line with this, recent studies have shown that ERα-targeting PROTACs can also effectively degrade ERα and combat endocrine-resistant breast cancer[61,62]. In our study, we observed high ERα expression in samples from patients with endocrine treatment relapse, aligning with previous findings. Moreover, as a molecular glue of ERα, Bufalin exhibited potent anti-cancer effects in vitro, in vivo, and in Tamoxifen-resistant patient-derived organoids. By degrading ERα, Bufalin has the potential to reverse Tamoxifen resistance, offering a promising therapeutic strategy for patients with limited treatment options.

In summary, our study demonstrates that Bufalin selectively binds to the R394 residue of ERα and promotes its degradation based on the AI-driven methods. Additionally, Bufalin functions as a molecular glue, facilitating the interaction between ERα and the ubiquitin E3 ligase STUB1, ultimately leading to proteasomal degradation of ERα. Furthermore, Bufalin exhibits potent anti-cancer activity against Tamoxifen-resistant breast cancer in both preclinical models and patient-derived organoids. Collectively, our findings not only establish Bufalin as a molecular glue for ERα degradation but also highlight its potential as a promising lead compound for the treatment of Tamoxifen resistance.

Methods

Ethics approval

The experiments were approved by the Medical Ethics Review Committee of Xiangya Hospital of Central South University (Ethics code: 2023121169). Tissue samples were collected from the Xiangya Hospital of Central South University (Changsha, China), and all individuals provided informed consent prior to participating in the study.

Animal studies were approved by the Institutional Animal Care and Use Committee (IACUC) of Central South University (CSU-2023-0462), and all procedures were conducted in accordance with the institutional guidelines of the Animal Care and Use Committee of Central South University. All mice were housed in the Laboratory Animal Research Center of Central South University, which is a pathogen-free animal facility at a controlled temperature under standard laboratory conditions (12 h light/dark cycle, temperature kept at 21–24 °C and 40–70% humidity) with food and water provided ad libitum. Female mice were selected because the study focuses on breast cancer, a disease that predominantly affects females and is influenced by female-specific hormonal and physiological factors. In compliance with ethical regulations, tumor volume did not exceed 2000 mm^3, and no single tumor dimension exceeded 20 mm in diameter.

Target prediction of Bufalin based on an integrated multi-predictive strategy

To refine the target prediction range, we trained a deep learning model based on the Chemprop[25] package using binding data from 11 targets sourced from ChEMBL and PubChem, with an average of 1187 compounds per target (Supplementary Table 2). The dataset was randomly split into an 80% training set and a 20% test set.

The model employs a Graph Neural Network (GNN) architecture specifically designed to learn molecular representations from graph-structured data. It consists of four primary components: (1) a shared local feature encoder that extracts atom and bond features across all tasks; (2) a directed message-passing process that propagates information along directed edges to generate atom embeddings; (3) an aggregation module that combines atom embeddings into a single molecular representation using sum or mean pooling; and (4) a feed-forward network (FFN) with task-specific multi-layer perceptron (MLP) layers to map molecular embeddings to target properties, enabling efficient multi-task predictions.

The model was trained with the Adam optimizer, incorporating learning rate scheduling, dropout regularization, and a model-ensembling strategy. Together with an advanced GNN architecture and a carefully curated dataset, this results in a robust and high-performing model, achieving a receiver operating characteristic area under the curve (ROC-AUC) of 0.94 on the test set (Supplementary Table 3). Finally, a default probability threshold of 0.8 was applied, ensuring that only targets meeting this performance criterion were selected.

Cell lines and culture

All cell lines were maintained at 37 °C in a humidified atmosphere of 5% CO_2/95% air. MCF-7 cells were purchased from Cell Bank (Chinese Academy of Sciences, Beijing, China). The T47D and 293 T cell lines were purchased from Cell Bank (Chinese Academy of Sciences, Shanghai, China). The Tamoxifen-resistant cells LCC2 were derived from Wuhan University. MCF-7 and 293 T cells were cultured in Dulbecco's Modified Eagle Medium (DMEM) (Gibco, Carlsbad, CA, USA) with 10% Fetal Bovine Serum and 1% penicillin streptomycin. T47D were cultured in RPMI-1640 medium

https://doi.org/10.1038/s41467-025-62288-7

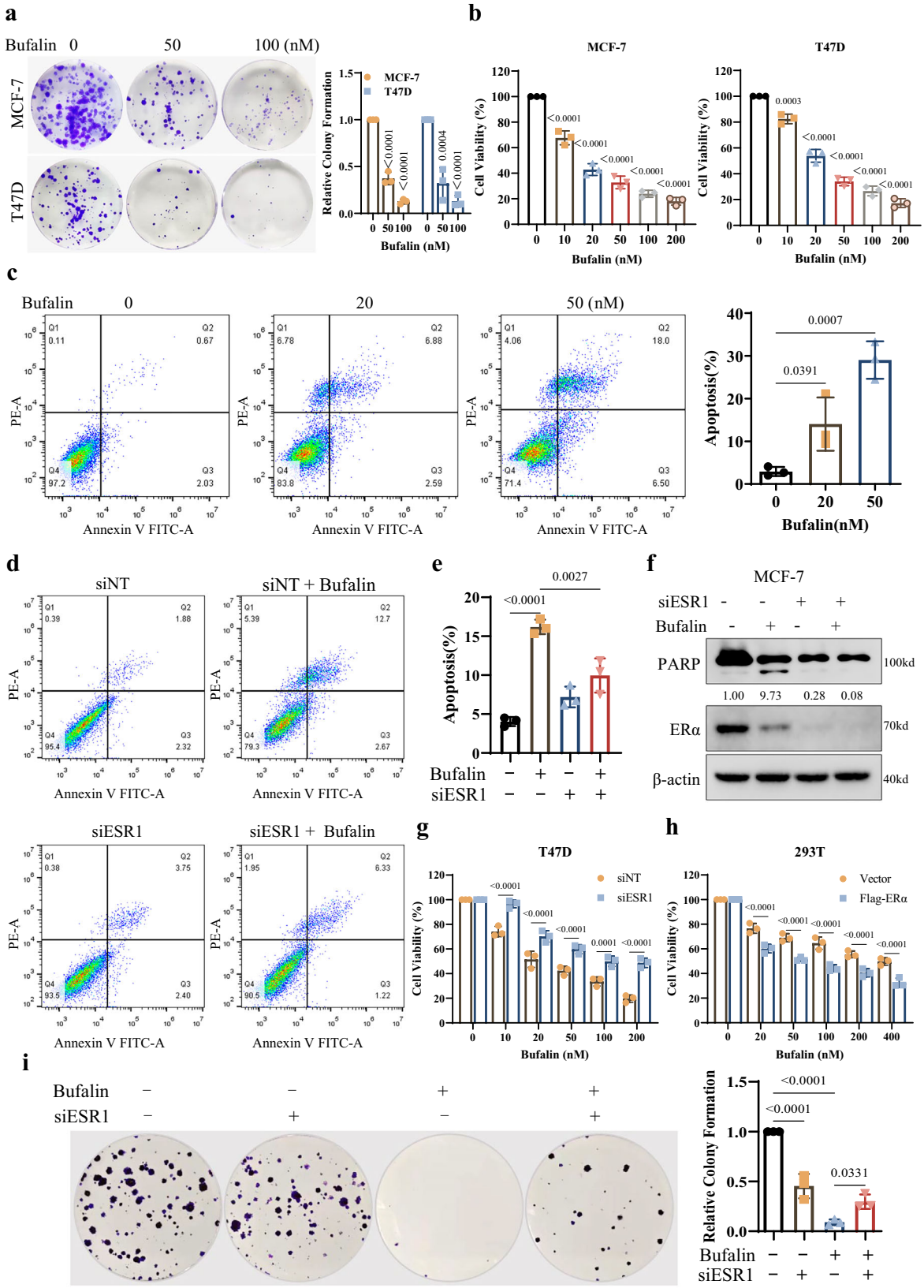

(Gibco, Carlsbad, CA, USA) with 10% Fetal Bovine Serum and 1% penicillin streptomycin. Tamoxifen-resistant LCC2 cells were cultured according to the literature[52], briefly, LCC-2 cell lines were cultured in RPMI-1640 medium (10% Fetal Bovine Serum and 1% penicillin streptomycin). All cell lines were tested negative for mycoplasma contamination.

Reagents and Antibodies

Bufalin was purchased from APExBIO (USA). Fulvestrant, Estradiol (E2), and MG-132 were purchased from MedChemExpress (Monmouth Junction, NJ, USA). MLN4924 was purchased from TargetMol (Washington, USA). The recombinant Human CYP17A1 (cat. no. CSB-EP006392HU) and estrogen receptor (ESR1) (Cat. no.

Fig. 6 | Bufalin's anti-cancer effects in ER+ cells are dependent on ERα. a The colony formation assay was used to measure MCF-7 and T47D cell proliferation after treatment by Bufalin, the data are presented as mean ± SD, n = 3 independent experiments. One-way ANOVA was used for statistical analysis, $P < 0.05$ was considered to be statistically significant. **b** MCF-7 and T47D cells were treated with a series of concentrations of Bufalin, and cell viability was determined using the CCK-8 assay, the data are presented as mean ± SD, n = 3 independent experiments. One-way ANOVA was used for statistical analysis, $P < 0.05$ was considered to be statistically significant. **c** MCF-7 cells were treated with 20 or 50 nM Bufalin for 48 h, and the apoptosis was examined by measuring Annexin V staining, the data are presented as mean ± SD, $n = 3$ independent experiments. One-way ANOVA was used for statistical analysis, $P < 0.05$ was considered to be statistically significant. **d**, **e** MCF-7 cells were transfected with nontargeting siRNA or ESR1 siRNA followed by treatment with Bufalin for 48 h, and apoptosis was examined by measuring Annexin V staining, the data are presented as mean ± SD, $n = 3$ independent experiments. One-way ANOVA was used for statistical analysis, $P < 0.05$ was considered to be statistically significant. **f** MCF-7 cells were transfected with nontargeting siRNA or ESR1 siRNA followed by treatment with Bufalin for 48 h, and the ERα and PARP protein levels were measured by western blot, the samples derive from the same experiment and that gels/blots were processed in parallel. **g** T47D cells were transfected with nontargeting siRNA or ESR1 siRNA followed by treatment with Bufalin, and the cell viability was determined using the CCK-8 assay, the data are presented as mean ± SD, $n = 3$ independent experiments. Two-way ANOVA was used for statistical analysis, $P < 0.05$ was considered to be statistically significant. **h** 293 T cells were transfected with Flag-ERα plasmid followed by treatment with Bufalin, and the cell viability was determined using the CCK-8 assay, the data are presented as mean ± SD, $n = 3$ independent experiments. Two-way ANOVA was used for statistical analysis, $P < 0.05$ was considered statistically significant. **i** MCF-7 cells were transfected with nontargeting siRNA or ESR1 siRNA followed by treatment with Bufalin, and the colony formation assay was used to measure cell proliferation, the data are presented as mean ± SD, $n = 3$ independent experiments. One-way ANOVA was used for statistical analysis, $P < 0.05$ was considered to be statistically significant.

CSB-YP007830HU) proteins were purchased from CUSABIO. Recombinant human PKC delta protein (ab60844) was purchased from Abcam (Cambridge, UK). Antibodies targeting ERα (Cat. no. 8644, WB, 1:1000), LC3 (Cat. no. 12741, WB,1:1000), PARP (Cat. no. 9532, WB,1:1000), and Bcl-2 (Cat. no.15071, WB, 1:1000) were purchased from Cell Signaling Technology (Danvers, MA, USA). The ERα (cat. no. 84564-4-RR, IHC, 1:500, IF, 1:250), STUB1 (Cat. no. 68407-1-Ig, WB, 1:1000), and β-actin (Cat. no. 81115-1-RR, WB, 1:5000) antibodies were purchased from Proteintech (Chicago, IL, USA). The Flag (cat. no. M185, WB, 1:1000) and HA antibodies (cat. no. M180, WB, 1:1000) were purchased from MBL (Tokyo, Japan), while the antibody against ubiquitin (cat. no. sc-8017, WB, 1:200) was purchased from Santa Cruz Biotechnology. Anti-mouse and anti-rabbit secondary antibodies were purchased from Abiowell (Shanghai, China). Streptavidin FITC (Cat. no. 11-4317-87) was purchased from Thermo Fisher Scientific (Waltham, MA, USA). Magnetic streptavidin beads (cat. no. 22305-1) were purchased from Beaver (Suzhou, China). Lipofectamine 8000 was purchased from Beyotime Biotechnology (Shanghai, China). Lipofectamine™ RNAiMAX was purchased from Invitrogen. Protein A/G agarose beads (cat. no. 10121) were obtained from Santa Cruz Biotechnology, and the CCK-8 was purchased from Bimake (Shanghai, China). An enhanced chemiluminescence kit (cat. no. BL520A) was purchased from BioSharp (Shanghai, China).

Plasmid and siRNA transfection

Plasmids encoding wild-type and mutant ERα were obtained from Gene (Shanghai, China), while siRNAs targeting ESR1 and STUB1 were purchased from GenePharma (Suzhou, China). The target sequence of ESR1 siRNA was as follows: GCACCCUCUUGUAUUCCUATT (sense), UAGGAAUACAAGAGGGUGCTT (antisense). The target sequence of STUB1 siRNA was as follows: GCAGUCUGUGAAGGCGCACTT (sense), GUGCGCCUUCACAGACUGCTT (antisense). For siRNA transfection, the siRNA targeting ESR1 or STUB1 was incubated with Lipofectamine™ RNAiMAX in serum-free medium according to the manufacturer's instructions. The plasmid was transfected using the Lipofectamine 8000 reagent in serum-free DMEM, according to the manufacturer's instructions.

Western Blot

After treatment, the cells were washed twice with cold PBS and lysed on ice for 30 minutes in RIPA lysis (Abiowell) supplemented with a protease inhibitor cocktail (Biotool), followed by centrifugation at 12,000 *g* for 15 minutes at 4 °C. The protein concentration of the supernatant was determined using BCA. Proteins were resolved by SDS-PAGE and then transferred to PVDF membrane (Merck KGaA, Darmstadt, Germany). The PVDF membranes were blocked with 5% skim milk for 1 h at room temperature and then incubated with the respective antibodies at 4 °C for 14 h. After 14 h the PVDF membranes were washed thrice with PBST and incubated with a secondary antibody at room temperature for 1 h. The signals were detected by chemiluminescence assay using a ChemiDoc Touch (Bio-Rad).

Cell viability assays

Briefly, cells were seeded into 96-well plates at an appropriate density and allowed to adhere overnight. The following day, cells were treated with various concentrations of the indicated drug and incubated for the desired time period. Subsequently, 10 μL of CCK-8 solution was added to each well and the plates were incubated at 37 °C for 1-2 hours. After incubation, absorbance was measured at 450 nm using a microplate reader.

Colony forming assay

MCF-7, T47D, and LCC2 cells were seeded in 6-well plates, exposed to the indicated treatments, and cultured for approximately 15 days, and the medium was changed every 3 days. After treatment, the cells were fixed with 4% paraformaldehyde, stained with crystal violet for 24 h, washed with water, and colonies were counted.

5-Ethynyl-2'- deoxyuridine Assay (EdU)

After treatment with Bufalin, LCC2 cells were incubated with 5-ethynyl-2'-deoxyuridine (EdU; RiboBio, Guangzhou, China) for 2 hours at 37 °C, according to the manufacturer's instructions. The cells were fixed with 4% paraformaldehyde at room temperature for 30 min, followed by treatment with 2 mg/mL glycine for 5 min. Next, the cells were permeabilized with 0.5% Triton X-100 for 10 min and stained with a 1× Apollo reaction cocktail for 30 min in the dark at room temperature. Finally, cell nuclei were counterstained with Hoechst 33342 for 30 min at room temperature. Images were captured using a fluorescence microscope.

Quantitative Real-time PCR

Total RNA was isolated from cells using the TRIzol reagent (CWBio, Taizhou, China), and reverse transcription was carried out using the PrimeScript RT reagent kit (TaKaRa, Japan) to generate complementary DNA (cDNA). Quantitative real-time PCR was conducted on a QuantStudio Real-Time PCR System (Life Technologies) using QuantStudio Design & Analysis Software v1.5.1. Gene expression levels were quantified using the standard $2^{-\Delta\Delta Ct}$ method. The qPCR primer sets were: ESR1: GGGAAGTATGGCTATGGAATCTG (forward), TGGCTGGACACATATAGTCGTT (reverse); AGR2: AGAGCAGTTTGTC CTCCTCAA (forward), CAGGTTCGTAAGCATAGAGACG (reverse); CCND1: CAATGACCCCGCACGATTTC (forward), CATGGAGGGCGGA TTGGAA (reverse); GREB1: TGGTCCGTAATGCACAAGGG (forward), CTGCGTTTAGTGAGGGGTGA (reverse); NRIP1: GGATCAGGTACTG

https://doi.org/10.1038/s41467-025-62288-7

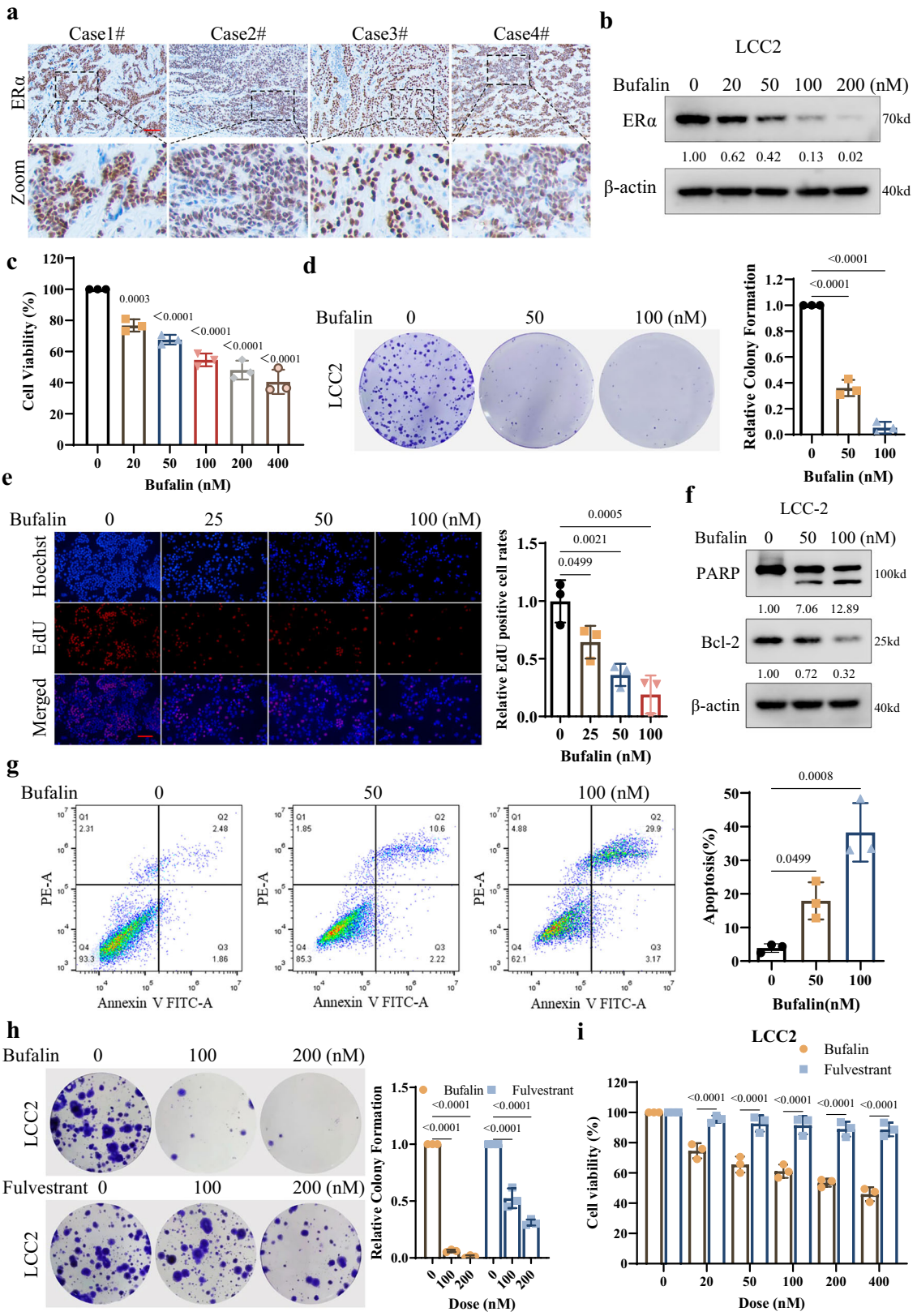

CCGTTGAC (forward), CTGGACCATTACTTTGACAGGTG (reverse); PGR: TTATGGTGTCCTTACCTGTGGG (forward), GCGGATTTTAT CAACGATGCAG (reverse); SIAH2: TCTTCGAGTGTCCGGTCTG (forward), CGGCATTGGTTACACACCAG (reverse), GAPDH: TGACATCAA-GAAGGTGGTGAAGCAG (forward), GTGTCGCTGTTGAAGTCAGAG GAG (reverse).

Flow-cytometric analysis of apoptosis

After Bufalin treatment, the cells were collected and washed twice with cold PBS. Subsequently, 5 μL Annexin V-FITC and 5 μL propidium iodide (PI) staining buffer were added to the cells and incubated in the dark at room temperature. After 15 min, the stained cells were analyzed using FACS.

Fig. 7 | Bufalin overcomes Tamoxifen resistance in vitro. a Representative IHC staining for ERα in Tamoxifen treatment relapsed simple (Scale bar 20μm). **b** Tamoxifen-resistant cells LCC2 were treated with a serious of Bufalin, the expression of ERα was measured by western blot. **c** Tamoxifen-resistant cells LCC2 were treated with Bufalin, and cell viability was determined using the CCK-8 assay, the data are presented as mean ± SD, n = 3 independent experiments. One-way ANOVA was used for statistical analysis, $P < 0.05$ was considered statistically significant. **d** The colony formation assay was used to measure LCC2 cell proliferation after treatment by Bufalin, the data are presented as mean ± SD, n = 3 independent experiments. One-way ANOVA was used for statistical analysis, $P < 0.05$ was considered to be statistically significant. **e** The EdU assay was used to measure LCC2 cell proliferation following treatment with Bufalin (Scale bar 100μm), the data are presented as mean ± SD, $n = 3$ independent experiments. One-way ANOVA was used for statistical analysis, $P < 0.05$ was considered statistically significant. **f** LCC2 cells were treated with 50 or 100 nM Bufalin for 48 h, and the expression of PARP and Bcl-2 was measured by western blot, the samples derive from the same experiment and that gels/blots were processed in parallel. **g** LCC2 cells were treated with 50 or 100 nM Bufalin for 48 h, and apoptosis was examined by measuring Annexin V staining, the data are presented as mean ± SD, $n = 3$ independent experiments. One-way ANOVA was used for statistical analysis, $P < 0.05$ was considered statistically significant. **h** The colony formation assay was used to measure LCC2 cell proliferation after treatment with Bufalin or Fulvestrant, the data are presented as mean ± SD, $n = 3$ independent experiments. One-way ANOVA was used for statistical analysis, $P < 0.05$ was considered statistically significant. **i** Tamoxifen-resistant cells LCC2 were treated with Bufalin and Fulvestrant, and cell viability was determined using the CCK-8 assay, the data are presented as mean ± SD, $n = 3$ independent experiments. Two-way ANOVA was used for statistical analysis, $P < 0.05$ was considered statistically significant.

Immunofluorescence staining

MCF-7 cells treated with Biotin-Bufalin on glass coverslips were fixed in 4% paraformaldehyde for 30 min at room temperature and blocked with 5% bovine serum albumin (BSA) for 1 h. The fixed cells were then incubated with anti-ERα antibody and streptavidin FITC at 4 °C overnight, followed by Alexa Fluor 594 anti-rabbit IgG antibody. At the end of the incubation period, the cells' nuclei were stained with DAPI, and the fluorescence signal was detected and captured using confocal microscopy.

Co-immunoprecipitation (Co-IP) assay

The 293 T cells were transiently transfected with Flag-ERα plasmid or HA-STUB1 and subjected to Bufalin treatment as indicated. After treatment, the cells were washed twice with PBS and lysed in mammalian protein extraction reagent buffer (cat. no. 78501; Thermo Scientific), supplemented with protease and phosphatase inhibitors for 30 min. Cell lysates were centrifuged, and supernatant was precleared with protein G agarose beads (Santa Cruz), then subjected to immunoprecipitation with indicated antibodies and protein A/G agarose beads at 4 °C overnight. The next day, the immunocomplexes were washed five times with PBS, and the binding proteins were eluted by 1 × SDS-PAGE loading buffer at 95 °C for 10 min. Bound proteins were identified using immunoblotting and western blot.

Biotin-pull down assay

After treatment, the cells were washed with PBS and lysed for 30 min in mammalian protein extraction (Thermo Scientific) with protease and phosphatase inhibitors. Following cell lysis, the supernatants were collected by centrifugation at 12,000 × g for 15 minutes at 4 °C. The streptavidin magnetic beads were pre-incubated with the cell lysate for 2 hours. Subsequently, 500 μg of clarified cell lysate was incubated with either D-Biotin or Biotin-Bufalin overnight at 4 °C for target protein capture. The following day, the mixture containing biotin and cell lysate was coupled with streptavidin magnetic beads (Beaver) for 2 hours at room temperature. The magnetic beads were then collected using a magnetic rack and washed six times to remove non-specifically bound proteins. Bound proteins were eluted by boiling in 1× SDS-PAGE loading buffer at 95 °C for 10 minutes, followed by detection via western blot analysis.

Animal studies

Briefly, the Tamoxifen-resistant cells LCC2 (2×10^6 cells) were subcutaneously injected into 4-week-old female nude mice (Hunan Slack Jingda Laboratory Animal Co., Ltd.). Tumor sizes were measured on different days after inoculation and calculated using the formula $V = lw^2\pi/6$, where l is the length and w is the width. When the tumors were palpable, the mice were randomly divided into designated groups and received the indicated treatments. The tumor volume was measured using a Vernier caliper every two days.

Immunohistochemistry (IHC)

The human cancer tissue specimens from patients with Tamoxifen treatment and recurrence, and animal tissue were fixed in 4% paraformaldehyde, embedded in paraffin, and sectioned at a thickness of 4 μm. After deparaffinization, antigen retrieval was performed using a citric acid buffer (pH 6.0). Endogenous peroxidase activity was blocked with 3% hydrogen peroxide, and following blocked with the application of normal serum. Sections were then incubated overnight at 4 °C with the antibodies against ERα and Ki67, followed by HRP-conjugated secondary antibodies. The signal was developed using DAB, and the nuclei were counterstained with hematoxylin. Immunohistochemical staining was performed according to the manufacturer's protocol.

Protein-ligand binding conformation modeling

The conformation of the protein-ligand complex was modeled using Schrödinger software (version 2022.1). The structure of Bufalin was obtained from PubChem, and ligand conformations were generated using LigPrep. The crystal structure of the ESR1 protein was obtained from the Protein Data Bank (PDB ID: 3ERT)[63]. The Glide SP protocol was employed to generate the optimal conformation of the protein-ligand complex.

Protein-protein docking conformation modeling

The structures of STUB1, TRIM56, RNF181, RNF2, and ESR1 proteins were obtained from the Protein Data Bank and Alphafold 3, and subjected to 15 repeats of optimization using the relax module of Rosetta (version 3.5.1)[64]. Ten conformations were generated from each optimization, and the top-scoring conformation from Rosetta was used for subsequent protein-protein docking. Initial protein-protein docking was performed using the ClusPro server[65]. Complex conformations with incorrect STUB1, TRIM56, RNF181, and RNF2 binding modes were excluded from the ClusPro docking results. These conformations were subjected to structural refinement using the docking protocol of Rosetta. All generated conformations were ranked according to their Rosetta scores.

Molecular dynamic simulations

Molecular simulations of ESR1-Bufalin, ESR1-STUB1, and ESR1-Bufalin-STUB1 complexes were conducted using Amber22 software. Proteins and ligands were parameterized using Amber ff19SB[66] and GAFF2[67] force fields, respectively. The complex systems were solvated in a TIP3P water box extending 10 Å from the protein. Chloride and sodium ions were then added to neutralize the system. Subsequently, energy minimization was performed for up to 20,000 steps. The systems were heated from 0 K to 298.15 K over 100 ps and the pressure was increased to atmospheric pressure over another 100 ps, with a time step of 1 fs during the heating and pressurization processes. Finally, a 200 ns production classical MD simulation was conducted with a time step of 2 fs. Trajectory analysis was performed using CPPTRAJ.

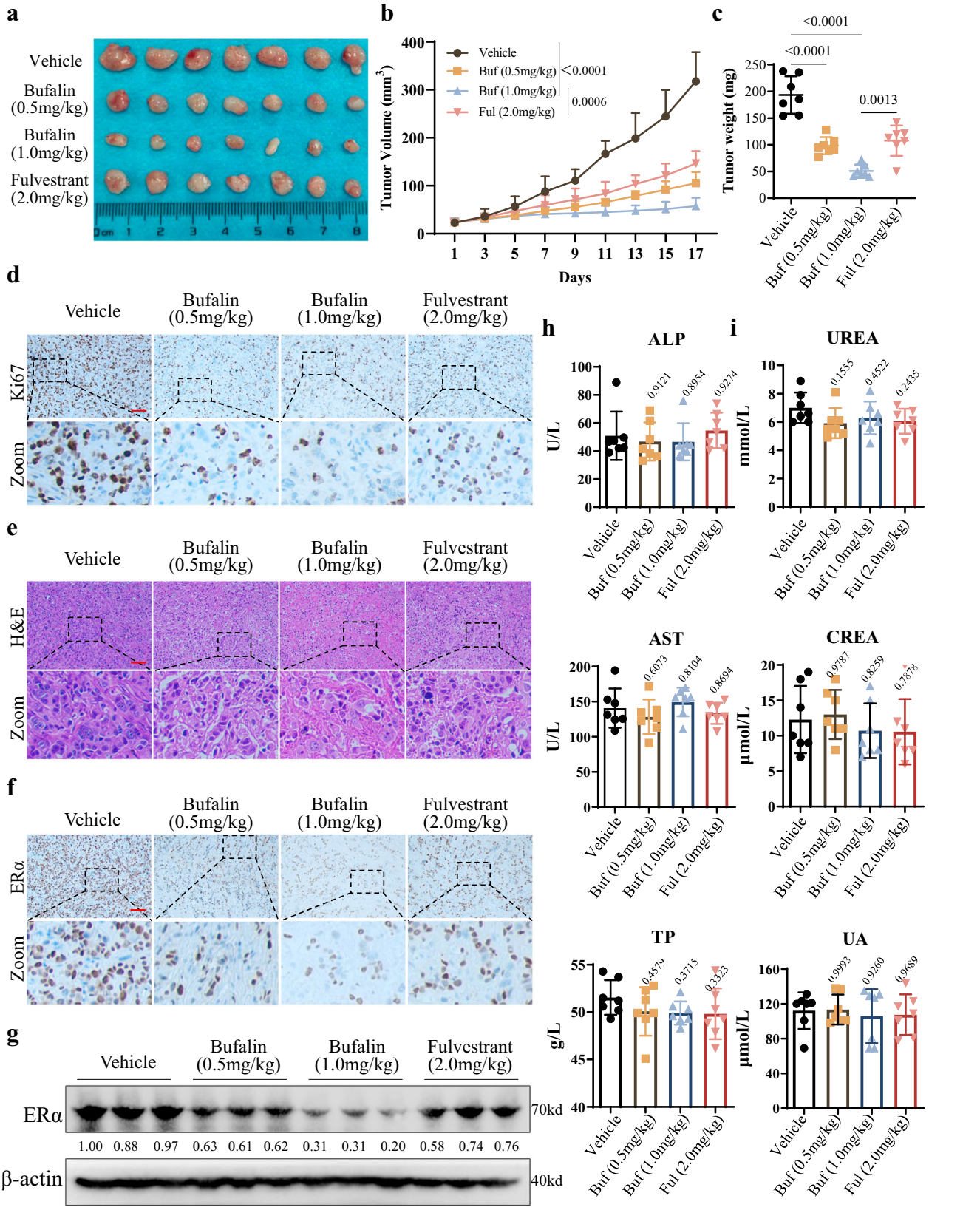

MM-PBSA and alanine scanning mutations analysis

MM-PBSA binding free energy calculations were performed using MMPBSA.py from AmberTools2023[68], using only the last 100 ns of the trajectory. We extracted 100 frames from the trajectory for subsequent energy calculations. In addition, residual energy decomposition was performed for the Bufalin-ESR1 complex. Alanine scanning mutations[69] were conducted on the top ten residues from the energy decomposition analysis.

Surface Plasmon Resonance (SPR) assay

After storage at -80 °C, Bufalin and the recombinant proteins CYP17A1, ESR1, and PKC delta were allowed to equilibrate to room temperature.

https://doi.org/10.1038/s41467-025-62288-7

Fig. 8 | Bufalin overcomes Tamoxifen resistance in vivo. 4-week-old female nude mice were inoculated with LCC2 cells. The tumor-bearing mice were subsequently given the indicated treatment ($n = 7$ mice per group). **a** Subcutaneous tumors were excised and photographed at the end of the experiment. **b** Tumor sizes were measured on the specified days, the data are presented as mean ± SD, $n = 7$ mice. One-way ANOVA was used for statistical analysis, $P < 0.05$ was considered to be statistically significant. **c** Tumor weights were measured at the end of the experiments, the data are presented as mean ± SD, $n = 7$ mice. One-way ANOVA was used for statistical analysis, $P < 0.05$ was considered to be statistically significant. **d** Representative IHC images for detecting Ki67 expression in the tumor specimens (Scale bar 20μm). **e** Representative histological analysis of tumor specimen stained by H&E (Scale bar 20μm). **f** Representative IHC images for detecting ERα expression in the tumor specimens (Scale bar 20μm). **g** Western blot analysis of the ERα protein expression in xenografts following the indicated treatment. **h**, **i** Mice liver and kidney functions were measured at the end of the experiments, the data are presented as mean ± SD, $n = 7$ mice. One-way ANOVA was used for statistical analysis, $P < 0.05$ was considered to be statistically significant (Vehicle vs. Buf (0.5 mg/kg), Vehicle vs. Buf (1.0 mg/kg), Vehicle vs. Ful (2.0 mg/kg)). Buf Bufalin, Ful Fulvestrant.

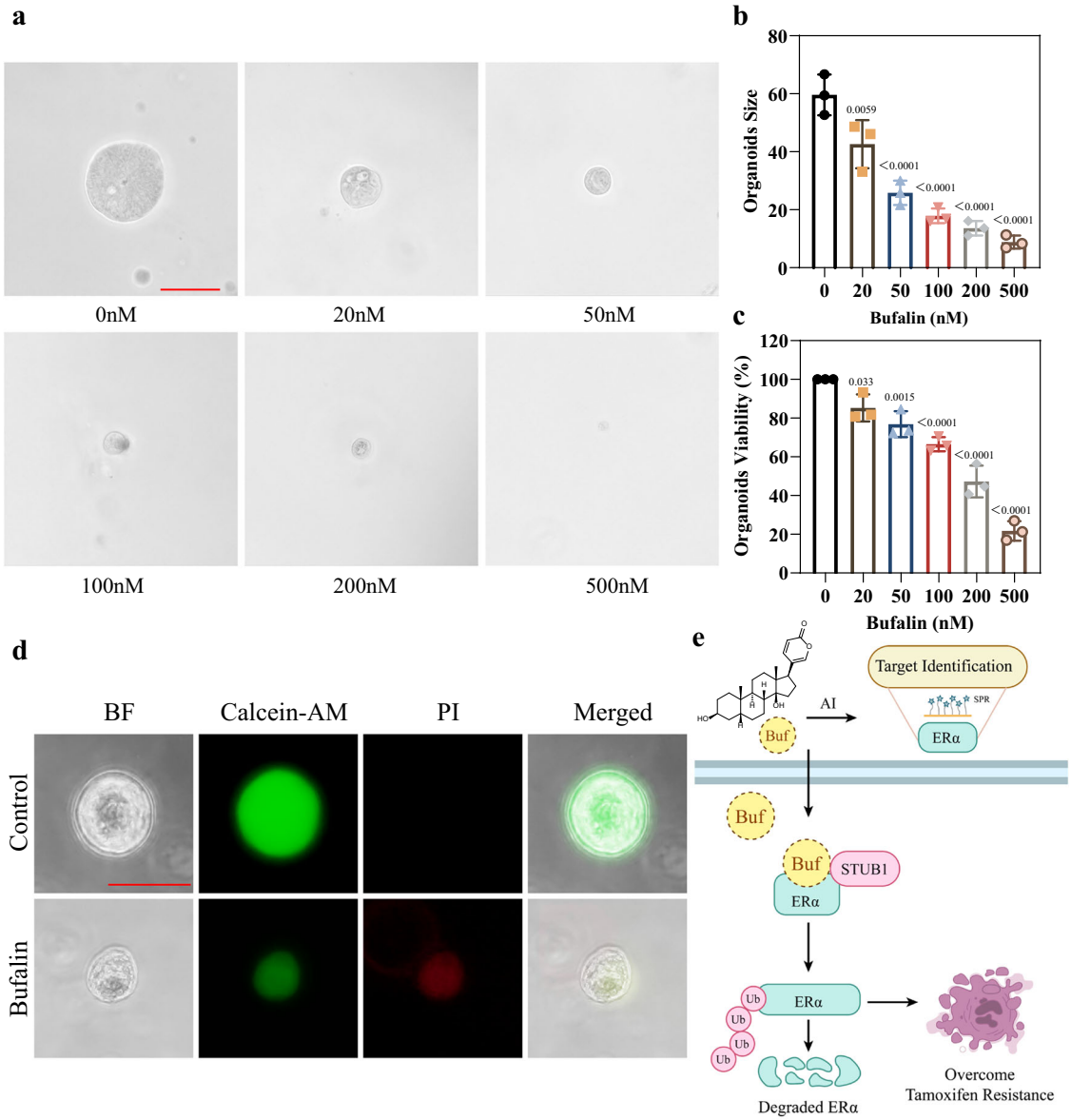

Fig. 9 | Bufalin exerts significant anti-cancer activity in Tamoxifen-resistant patient-derived organoids. a Representative images of Tamoxifen treatment relapsed patient-derived organoids after treatment by Bufalin (Scale bar 50 μm). Representative data are shown from n = 3 independent experiments with consistent results. **b** Statistics of tumor organoid size of formed organoids after Bufalin treatment, the data are presented as mean ± SD, $n = 3$ independent experiments. One-way ANOVA was used for statistical analysis, $P < 0.05$ was considered statistically significant. **c** The proliferation of Tamoxifen treatment relapsed patient-derived organoids treated with Bufalin, the data are presented as mean ± SD, $n = 3$ independent experiments. One-way ANOVA was used for statistical analysis, $P < 0.05$ was considered statistically significant. **d** The growth inhibition of Bufalin was demonstrated by Calcein-AM/PI fluorescence staining of PDO (Scale bar 50μm). BF: bright field. Representative data are shown from $n = 3$ independent experiments with consistent results. **e** Schematic of the proposed mechanism of Bufalin in ER-positive breast cancer. This study harnessed artificial intelligence combined with molecular docking to predict the molecular mechanism of Bufalin against tumor. Bufalin could bind to ERα and increase the interaction between ERα and the ubiquitin E3 ligase STUB1, leading to the degradation of ERα. Additionally, Bufalin could overcome Tamoxifen resistance in vitro and in vivo.

Bufalin was diluted with DMSO to the appropriate concentration for spotting and used as the immobilized phase. The working solution was printed onto a 3D photocrosslinkable sensor chip using the BioDot™ AD1520 microarray printer, with four nonadjacent replicate spots per compound. The printed chips were vacuum-dried and then subjected to UV-induced photocrosslinking using a crosslinking instrument. Following crosslinking, the chips were sequentially washed on a shaker with DMF, ethanol (EtOH), and deionized water for 15 minutes each. The recombinant protein samples were diluted to generate five concentration gradients: 200 nM, 400 nM, 800 nM, 1600 nM, and 3200 nM, and were injected over the chip surface. During interaction analysis, the protein analytes were passed over the chip surface at a flow rate of 0.5 μL/s. Each association phase lasted 600 seconds, followed by a 360-second dissociation phase. After each binding cycle, the chip surface was regenerated with 10 mM glycine-HCl (pH 2.0) at a flow rate of 2 μL/s to remove the bound analytes.

Patient-derived organoid

Tissue specimens from patients who relapsed after Tamoxifen therapy were processed for organoid culture according to previous protocols[70,71]. Samples were obtained from the Xiangya Hospital of Central South University (Changsha, China), and written informed consent was obtained from all participants prior to collection. Tissue samples were enzymatically digested into single-cell suspensions using collagenase (Sigma) and subsequently cultured in a 3D environment composed of 50% chilled Matrigel (Corning). After 5 days of culture, the resulting organoids were dissociated into single-cell suspensions, seeded into 384-well plates, and treated with Bufalin. After 4 days of treatment, cell viability was assessed using CellTiter-Glo 3D Reagent (Promega) according to the manufacturer's instructions.

Organoid live/dead cell staining

Live/dead organoid cell staining was performed as previously described[72]. Following treatment, the samples were washed twice with cold PBS and subsequently stained with Calcein-AM and propidium iodide (PI) at 37 °C for 20 minutes in the dark. Finally, the images were captured using a fluorescence microscope.

Statistics and reproducibility

We analyzed the data using GraphPad Prism 9.0 software. All samples represent biological replicates, and the statistical measurements are presented as mean ± SD as specified in each figure. No statistical method was used to predetermine sample size. No data were excluded from the analyses. The experiments were randomized. The Investigators were blinded to allocation during experiments and outcome assessment. Statistical analyses were performed using one-way or two-way ANOVA, depending on the experimental design. A P-value < 0.05 was considered statistically significant. The P values are given in the figures. All representative experiments are repeated at least three times independently with similar results.

Reporting summary

Further information on research design is available in the Nature Portfolio Reporting Summary linked to this article.

Data availability

All data are included within the article, supplementary information or source data file. Source data are provided with this paper.

Code availability

The code has been made available on GitHub (https://github.com/wei-xiao-ya/multi_task-NN, https://github.com/LiHui-CADD/pro1-pro2-lig/tree/master). The molecular docking and MD simulation data are available in the "InputFile" and "code" sections, respectively, at https://github.com/LiHui-CADD/pro1-pro2-lig/tree/master.

References

1. Zhang, H. et al. Bufalin targeting CAMKK2 inhibits the occurrence and development of intrahepatic cholangiocarcinoma through Wnt/β-catenin signal pathway. *J. Transl. Med.* **21**, 900 (2023).
2. Yu, Z. et al. Bufalin stimulates antitumor immune response by driving tumor-infiltrating macrophage toward M1 phenotype in hepatocellular carcinoma. *J. Immunother. Cancer* **10**, e004297 (2022).
3. Farooqi, A. A. et al. Bufalin-mediated regulation of cell signaling pathways in different cancers: spotlight on JAK/STAT, Wnt/β-Catenin, mTOR, TRAIL/TRAIL-R, and non-coding RNAs. *Molecules* **28**, 2231 (2023).
4. Chen, J. et al. Bufalin targets the SRC-3/MIF pathway in chemoresistant cells to regulate M2 macrophage polarization in colorectal cancer. *Cancer Lett.* **513**, 63–74 (2021).
5. Soumoy, L., Ghanem, G. E., Saussez, S. & Journe, F. Bufalin for an innovative therapeutic approach against cancer. *Pharm. Res.* **184**, 106442 (2022).
6. Qian, Z. et al. Bufalin inhibits the proliferation of lung cancer cells by suppressing Hippo-YAP pathway. *Cell Signal* **109**, 110746 (2023).
7. Chen, G. et al. Bufalin targeting BFAR inhibits the occurrence and metastasis of gastric cancer through PI3K/AKT/mTOR signal pathway. *Apoptosis* **28**, 1390–1405 (2023).
8. Wang, Y. et al. Bufalin is a potent small-molecule inhibitor of the steroid receptor coactivators SRC-3 and SRC-1. *Cancer Res.* **74**, 1506–1517 (2014).
9. Qiu, Y. & Cheng, F. Artificial intelligence for drug discovery and development in Alzheimer's disease. *Curr. Opin. Struct. Biol.* **85**, 102776 (2024).
10. Pun, F. W., Ozerov, I. V. & Zhavoronkov, A. AI-powered therapeutic target discovery. *Trends Pharm. Sci.* **44**, 561–572 (2023).
11. Wei, H. et al. A combinatorial target screening strategy for deorphaning macromolecular targets of natural product. *Eur. J. Med. Chem.* **204**, 112644 (2020).
12. Cao, D. S. et al. A multi-scale systems pharmacology approach uncovers the anti-cancer molecular mechanism of Ixabepilone. *Eur. J. Med. Chem.* **199**, 112421 (2020).
13. Wei, X. et al. Predicting novel targets with Bayesian machine learning by integrating multiple biological signatures. *Chem. Sci.* **15**, 14471–14484 (2024).
14. Deng, X. et al. Identification of Novel Dual-Target Estrogen Receptor α Degraders with Tubulin inhibitory activity for the treatment of endocrine-resistant breast cancer. *J. Med Chem.* **66**, 11094–11117 (2023).
15. Zhao, W. et al. Ginsenoside Rg3 overcomes tamoxifen resistance through inhibiting glycolysis in breast cancer cells. *Cell Biol. Int.* **48**, 496–509 (2024).
16. Yuan, J. et al. Tinagl1 restores tamoxifen sensitivity and blocks fibronectin-induced EMT by simultaneously blocking the EGFR and β1-integrin/FAK signaling pathways in tamoxifen-resistant breast cancer cells. *IUBMB Life* **77**, e2940 (2025).
17. Kumar, N. et al. Most recent strategies targeting estrogen receptor alpha for the treatment of breast cancer. *Mol. Divers* **25**, 603–624 (2021).
18. Burstein, H. J. Systemic Therapy for Estrogen Receptor-Positive, HER2-Negative Breast Cancer reply. *Reply, N. Engl. J. Med.* **384**, 1176–1177 (2021).
19. Zhou, J. et al. A novel selective estrogen receptor degrader induces cell cycle arrest in breast cancer via ERα degradation and the autophagy-lysosome pathway. *Bioorg. Med. Chem.* **82**, 117235 (2023).
20. Zheng, Z. Z. et al. Super-enhancer-controlled positive feedback loop BRD4/ERα-RET-ERα promotes ERα-positive breast cancer. *Nucleic Acids Res.* **50**, 10230–10248 (2022).
21. Chen, X. S. et al. UCH-L1-mediated Down-regulation of Estrogen Receptor α Contributes to Insensitivity to Endocrine Therapy for Breast Cancer. *Theranostics* **10**, 1833–1848 (2020).

22. Liu, S. et al. MCM2 is involved in subtyping and tamoxifen resistance of ERα-positive breast cancer by acting as the downstream factor of ERα,. *Biotechnol. J.* **19**, e2300560 (2024).
23. Lai, X. et al., HGF/c-Met Promotes Breast Cancer Tamoxifen Resistance Through the EZH2/HOTAIR-miR-141/200a Feedback Signaling Pathway. *Mol. Carcinog.* **64**, 769–783 (2025).
24. Melone, V. et al. LncRNA PVT1 links estrogen receptor alpha and the polycomb repressive complex 2 in suppression of pro-apoptotic genes in hormone-responsive breast cancer. *Cell Death Dis.* **16**, 80 (2025).
25. Heid, E. et al. Chemprop: A Machine Learning Package for Chemical Property Prediction. *J. Chem. Inf. Model* **64**, 9–17 (2024).
26. Su, S., Dou, H., Wang, Z. & Zhang, Q. Bufalin inhibits ovarian carcinoma via targeting mTOR/HIF-α pathway. *Basic Clin. Pharm. Toxicol.* **128**, 224–233 (2021).
27. Yu, Z. et al. Bufalin inhibits hepatitis B virus-associated hepatocellular carcinoma development through androgen receptor dephosphorylation and cell cycle-related kinase degradation. *Cell Oncol.* **43**, 1129–1145 (2020).
28. Chen, R. Y. et al. Estradiol inhibits Th17 cell differentiation through inhibition of RORγT transcription by recruiting the ERα/REA complex to estrogen response elements of the RORγT promoter. *J. Immunol.* **194**, 4019–4028 (2015).
29. Casa, A. J., Hochbaum, D., Sreekumar, S., Oesterreich, S. & Lee, A. V. The estrogen receptor alpha nuclear localization sequence is critical for fulvestrant-induced degradation of the receptor. *Mol. Cell Endocrinol.* **415**, 76–86 (2015).
30. Yuan, L., Li, X., Yang, H. & Li, H. The ubiquitin ligase RNF2 stabilizes ERα and modulates breast cancer progression. *Hum. Cell* **36**, 353–365 (2023).
31. Zhu, J. et al. The ubiquitin ligase RNF181 stabilizes ERα and modulates breast cancer progression. *Oncogene* **39**, 6776–6788 (2020).
32. Xue, M. et al. Regulation of estrogen signaling and breast cancer proliferation by an ubiquitin ligase TRIM56. *Oncogenesis* **8**, 30 (2019).
33. Fan, M., Park, A. & Nephew, K. P. CHIP (carboxyl terminus of Hsc70-interacting protein) promotes basal and geldanamycin-induced degradation of estrogen receptor-alpha. *Mol. Endocrinol.* **19**, 2901–2914 (2005).
34. McDonough, H. & Patterson, C. CHIP: a link between the chaperone and proteasome systems. *Cell Stress Chaperones* **8**, 303–308 (2003).
35. Luo, H., Liu, N. & Lin, C. Dopamine enhances recovery after traumatic brain injury through ubiquitylation and autophagic degradation of RIPK1. *Cell Commun. Signal* **22**, 134 (2024).
36. Shomali, M. et al. SAR439859, a Novel Selective Estrogen Receptor Degrader (SERD), demonstrates effective and broad antitumor activity in wild-type and mutant ER-Positive breast cancer models. *Mol. Cancer Ther.* **20**, 250–262 (2021).
37. Ye, Q. et al. An overview of the past decade of bufalin in the treatment of refractory and drug-resistant cancers: current status, challenges, and future perspectives. *Front. Pharm.* **14**, 1274336 (2023).
38. Zhang, Z., He, X., Long, D., Luo, G. & Chen, S. Enhancing generalizability and performance in drug-target interaction identification by integrating pharmacophore and pre-trained models. *Bioinformatics* **40**, i539–i547 (2024).
39. Song, W., Xu, L., Han, C., Tian, Z. & Zou, Q. Drug-target interaction predictions with multi-view similarity network fusion strategy and deep interactive attention mechanism. *Bioinformatics* **40**, btae346 (2024).
40. Lin, X., Li, X. & Lin, X. A Review on Applications of Computational Methods in Drug Screening and Design. *Molecules* **25**, 1375 (2020).
41. Jiang, S. L. et al. Tubeimoside-1, a triterpenoid saponin, induces cytoprotective autophagy in human breast cancer cells in vitro via Akt-mediated pathway. *Acta Pharm. Sin.* **40**, 919–928 (2019).
42. Guan, Y. et al. Combined treatment of mitoxantrone sensitizes breast cancer cells to rapalogs through blocking eEF-2K-mediated activation of Akt and autophagy. *Cell Death Dis.* **11**, 948 (2020).
43. Wang, T. et al. The effects of bufadienolides on HER2 overexpressing breast cancer cells. *Tumour Biol.* **37**, 7155–7163 (2016).
44. Wu, S. et al. Bufalin induces ferroptosis by modulating the 2,4-dienoyl-CoA reductase (DECR1)-SLC7A11 axis in breast cancer. *Phytomedicine* **135**, 156130 (2024).
45. Li, C. et al. Bufalin Ameliorates Myocardial Ischemia/Reperfusion Injury by Suppressing Macrophage Pyroptosis via P62 Pathway. *J. Cardiovasc. Transl. Res.* **18**, 221–236 (2024).
46. Zheng, Y. D. et al. Bufalin induces apoptosis and autophagy via the Ca2+/CaMKKβ/AMPK/Beclin1 signaling pathway in osteosarcoma cells. *Cell Biol. Int.* **47**, 1344–1353 (2023).
47. Liu, X. D., Song, C. Y., Kong, C. C. & Tian, X. Bufalin Induces Programmed Necroptosis in Triple-Negative Breast Cancer Drug-Resistant Cell Lines through RIP1/ROS-Mediated Pathway. *Chin. J. Integr. Med.* **28**, 900–908 (2022).
48. Zhang, Y. et al. Role of P53-Senescence induction in suppression of LNCaP prostate cancer growth by cardiotonic compound bufalin. *Mol. Cancer Ther.* **17**, 2341–2352 (2018).
49. Liu, T. et al. Bufalin inhibits cellular proliferation and cancer stem cell-like phenotypes via upregulation of MiR-203 in Glioma. *Cell Physiol. Biochem.* **44**, 671–681 (2017).
50. Chen, P., Li, B. & Ou-Yang, L. Role of estrogen receptors in health and disease. *Front Endocrinol.***13**, 839005 (2022).
51. Bak, M. J., Das Gupta, S., Wahler, J. & Suh, N. Role of dietary bioactive natural products in estrogen receptor-positive breast cancer. *Semin Cancer Biol.* **40-41**, 170–191 (2016).
52. Wang, Y. et al. Discovery of novel covalent selective estrogen receptor degraders against endocrine-resistant breast cancer. *Acta Pharm. Sin. B.* **13**, 4963–4982 (2023).
53. Békés, M., Langley, D. R. & Crews, C. M. PROTAC targeted protein degraders: the past is prologue. *Nat. Rev. Drug Discov.* **21**, 181–200 (2022).
54. Lemaitre, T. et al. Molecular glue degraders: exciting opportunities for novel drug discovery. *Expert Opin. Drug Discov.* **19**, 433–449 (2024).
55. Schreiber, S. L. The Rise of Molecular Glues. *Cell* **184**, 3–9 (2021).
56. Liu, T. T. et al. Atypical E3 ligase ZFP91 promotes small-molecule-induced E2F2 transcription factor degradation for cancer therapy. *EBioMedicine* **86**, 104353 (2022).
57. Zhu, J. et al. Involvement of RFC3 in tamoxifen resistance in ER-positive breast cancer through the cell cycle. *Aging* **15**, 13738–13752 (2023).
58. Song, T. et al. Small molecule inhibitor targeting the Hsp70-Bim protein-protein interaction in estrogen receptor-positive breast cancer overcomes tamoxifen resistance. *Breast Cancer Res.* **26**, 33 (2024).
59. Hanker, A. B., Sudhan, D. R. & Arteaga, C. L. Overcoming endocrine resistance in breast cancer. *Cancer Cell* **37**, 496–513 (2020).
60. Lu, Y. & Liu, W. Selective Estrogen Receptor Degraders (SERDs): A promising strategy for estrogen receptor positive endocrine-resistant breast cancer. *J. Med Chem.* **63**, 15094–15114 (2020).
61. Xie, B. et al. Discovery of a novel class of PROTACs as potent and selective estrogen receptor α degraders to overcome endocrine-resistant breast cancer in vitro and in vivo. *J. Med Chem.* **66**, 6631–6651 (2023).
62. Deng, X. et al. Discovery of novel bicyclic phenylselenyl-containing hybrids: an orally bioavailable, potential, and multiacting class of estrogen receptor modulators against endocrine-resistant breast cancer. *J. Med Chem.* **65**, 7993–8010 (2022).

63. Shiau, A. K. et al. The structural basis of estrogen receptor/coactivator recognition and the antagonism of this interaction by tamoxifen. *Cell* **95**, 927–937 (1998).
64. Ó Conchúir, S. et al. A web resource for standardized benchmark datasets, metrics, and rosetta protocols for macromolecular modeling and design. *PLoS One*. **10**, e0130433 (2015).
65. Alekseenko, A., Ignatov, M., Jones, G., Sabitova, M. & Kozakov, D. Protein-protein and protein-peptide docking with ClusPro server. *Methods Mol. Biol.* **2165**, 157–174 (2020).
66. Tian, C. et al. ff19SB: Amino-acid-specific protein backbone parameters trained against quantum mechanics energy surfaces in solution. *J. Chem. Theory Comput*. **16**, 528–552 (2020).
67. Wang, J., Wolf, R. M., Caldwell, J. W., Kollman, P. A. & Case, D. A. Development and testing of a general amber force field. *J. Comput Chem*. **25**, 1157–1174 (2004).
68. Case, D. A. et al. AmberTools. *J. Chem. Inf. Model* **63**, 6183–6191 (2023).
69. Miller, B. R. 3rd et al. MMPBSA.py: An Efficient Program for End-State Free Energy Calculations. *J. Chem. Theory Comput*. **8**, 3314–3321 (2012).
70. Wan, X. et al. Identification of a Novel Substrate for eEF2K and the AURKA-SOX8 as the Related Pathway in TNBC. *Adv. Sci.* **12**, e2412985 (2025).
71. Jiang, T. et al. Targeting lncRNA DDIT4-AS1 Sensitizes Triple Negative Breast Cancer to Chemotherapy via Suppressing of Autophagy. *Adv. Sci.* **10**, e2207257 (2023).
72. Gong R. et al. GPX4-AUTAC induces ferroptosis in breast cancer by promoting the selective autophagic degradation of GPX4 mediated by TRAF6-p62, *Cell Death Differ*. https://doi.org/10.1038/s41418-025-01528-1. Online ahead of print (2025).

Acknowledgements

We gratefully acknowledge Professor Ceshi Chen (Kunming Medical University) for generously providing the HA-STUB1 plasmid, and Professor Haibing Zhou (Wuhan University) for the kind gift of the Tamoxifen-resistant LCC2 cell line. This work was supported by National Key Research and Development Program of China (2021YFF1201400 to DS C), the National Natural Science Foundation of China (22173118 to DS C, 82304553 to SL J), the Science and Technology Innovation Program of Hunan Province (2021RC4011 to DS C), Hunan Provincial Leading Talents in Scientific and Technological Innovation (Top Tier) Program (2022RC3076 to Y C), the Natural Science Foundation of Hunan Province (2022JJ80104 to DS C, 2023JJ40952 to SL J), the Natural Science Foundation of Changsha Municipal (kq2208407 to SL J), Talent Project Established by Chinese Pharmaceutical Association Hospital Pharmacy Department (CPA-Z05-ZC-2023-003 to SL J). We acknowledge Haikun Xu, Ph.D, and the High-Performance Computing Center of Central South University for support.

Author contributions

Y.C. and D.S.C. designed the study and revised the manuscript. S.L.J., T.J., X.W., X.Y.W., R.G., and C.X.Z. performed the experiments and analyzed the experimental data. H.L. conducted molecular docking experiments. S.L.J., K.Y.L., and T.J. drafted the manuscript. Z.L.C., C.Z., and Q.Z. helped with data analysis.

Competing interests

The authors declare no competing interests.

Additional information

Supplementary information The online version contains supplementary material available at https://doi.org/10.1038/s41467-025-62288-7.

Correspondence and requests for materials should be addressed to Yan Cheng or Dongsheng Cao.

Peer review information *Nature Communications* thanks Tao Zhu, Shirley Siu, Hui Yu, and the other anonymous, reviewer(s) for their contribution to the peer review of this work. A peer review file is available.